



CORAL: Correspondence Alignment for Improved Virtual Try-On

Jiyoung Kim¹ Youngjin Shin¹ Siyoon Jin¹ Dahyun Chung¹ Jisu Nam¹ Tongmin Kim¹
 Jongjae Park² Hyeonwoo Kang² Seungryong Kim¹

<https://cvlab-kaist.github.io/CORAL>



Figure 1. Teaser. (a) CORAL is a Diffusion Transformer-based framework that explicitly enhances person→garment correspondence within the 3D attention of DiT. This leads to more accurate local details in the generated results, such as fewer artifacts like duplicated garment hems, as shown in the baseline. (b) Virtual Try-On results on VITON-HD and DressCode, comparing outputs without and with CORAL. (c) Person-to-Person garment transfer results on PPR10K in challenging in-the-wild images.

Abstract

Existing methods for Virtual Try-On (VTON) often struggle to preserve fine garment details, especially in unpaired settings where accurate person–garment correspondence is required. These methods do not explicitly enforce person–garment alignment and fail to explain how correspondence emerges within Diffusion Transformers (DiTs). In this paper, we first analyze full 3D attention in DiT-based architecture and reveal that the person→garment correspondence critically depends on precise person→garment query–key matching within the full 3D attention. Building on this insight, we then introduce CORrespondence

ALignment (CORAL), a DiT-based framework that explicitly aligns query–key matching with robust external correspondences. CORAL integrates two complementary components: a correspondence distillation loss that aligns reliable matches with person→garment attention, and an entropy minimization loss that sharpens the attention distribution. We further propose a VLM-based evaluation protocol to better reflect human preference. CORAL consistently improves over the baseline, enhancing both global shape transfer and local detail preservation. Extensive ablations validate our design choices.

1. Introduction

Given a pair of person and garment images, Virtual Try-On (VTON) aims to synthesize the same person wearing the given garment, while handling large geometric variations

¹KAIST AI ²NC AI Co., Ltd. Correspondence to: Seungryong Kim <seungryong.kim@kaist.ac.kr>.



Figure 2. Correlation between Query-Key Matching and VTON Performance. Pink marker denotes the query points. (a) presents qualitative correlation between VTON performance and person→garment attention. All outputs in (a) are generated by the baseline. Human-preferred outputs show accurately localized, sharp attention, while low quality outputs show dispersed attention on incorrect locations. (b) reports quantitative correlation, where r denotes Pearson correlation coefficient. PCK of person→garment correspondence correlates with SSIM and LPIPS of the generated images, indicating that better localization predicts higher visual quality (Best viewed when zoomed-in).

between them, including differences in pose, silhouette, and garment type or shape (Choi et al., 2024; Zhou et al., 2024). Therefore, a key challenge in VTON is *establishing accurate correspondence between the person and the garment*, as inaccurate matching can lead to suboptimal VTON outputs, including distorted garment shapes, misplaced textures, or incorrect fitting.

Despite this challenge, most existing works focus on preserving fine-grained garment details through advanced inference techniques (Bhunia et al., 2023; Yang et al., 2024; Chong et al., 2025), additional conditioning signals (Choi et al., 2024; Kim et al., 2025; Xie et al., 2023), or garment encoders (Kim et al., 2023; Choi et al., 2024; Xu et al., 2024; Nam et al., 2025b), while often overlooking accurate person-garment matching. As a result, they still fail to faithfully transfer garment shape and local details (e.g., small logos or repetitive patterns), especially when given cross-category garments, where accurate matching is required.

Furthermore, most prior works (Zhou et al., 2024) are built upon diffusion U-Net architectures, with limited exploration of more advanced designs such as Diffusion Transformers (DiTs) (Peebles & Xie, 2023; Esser et al., 2024). Recent studies have shown that DiTs enable stronger in-context interactions between input tokens through full 3D attention (Tan et al., 2025a). This motivates us to develop DiT-based architectures for VTON to establish strong correspondence between person and garment input tokens.

To this end, we first analyze the behavior of full 3D attention in DiTs for VTON and reveal that *accurate person-garment alignment in RGB space critically depends on precise query-key correspondence within the 3D attention mechanism*. As illustrated in Fig. 1 and Fig. 2, we demonstrate that try-on quality linearly improves as the attention-derived matching between person queries and garment keys becomes more accurate.

Based on this analysis, we propose a novel DiT-based frame-

work, **COR**respondence **A**lignment (**CORAL**), which explicitly enhances person-garment correspondence by improving query-key matching in the full 3D attention of the DiT. Specifically, we introduce two complementary losses: (1) a **correspondence distillation loss** that aligns reliable matches obtained from the vision foundation model DiNOv3 (Siméoni et al., 2025) to person-garment query-key matching in the full 3D attention, and (2) an **entropy minimization loss** that sharpens the attention distribution by minimizing its entropy for localized and precise matching. We demonstrate the effectiveness of CORAL on standard VTON benchmarks in both paired and unpaired settings. To further evaluate the robustness of our method, we introduce a new evaluation dataset that includes real-world, challenging person-to-person unpaired scenarios. CORAL achieves state-of-the-art performance on SSIM, LPIPS, and FID across all benchmarks. We additionally evaluate our method using VLM-based assessment and human evaluation, achieving the best performance among all methods. Extensive ablation studies further validate our design choices. In summary, our contributions are as follows:

- We reveal that precise person-garment alignment in VTON critically depends on accurate query-key correspondence within the full 3D attention of DiTs.
- Based on these findings, we introduce CORAL, a DiT-based VTON framework that explicitly enhances person-garment correspondence through correspondence distillation and attention entropy minimization.
- We achieve consistent performance gains on standard metrics as well as human and VLM-based evaluations across VTON benchmarks, and validate our method on additional challenging settings that we introduce.

2. Related Works

Virtual Try-On. VTON aims to precisely transfer the shape and details of the garment image onto a person image. Several works improve sampling and alignment at inference (Bhunia et al., 2023; Chong et al., 2025; Wang et al., 2024; Li et al., 2025). Other efforts (Choi et al., 2024; Kim et al., 2025; Xie et al., 2023) add structural cues (e.g., parsing maps) to improve robustness against pose variations. Other methods inject global (Kim et al., 2023; Wan et al., 2024; Morelli et al., 2023) or local features (Choi et al., 2024; Zhou et al., 2024; Xu et al., 2024) from garment images to enhance detail preservation. Yet, they often lose garment details in unpaired settings that demand robust matching, leading to logo drift or boundary shifts.

Correspondence in Diffusion Models. The impressive performance of diffusion models comes from the rich visual representations they learn. Analyses of the internal attention mechanism in both UNet (Nam et al., 2024a;b; Jeong et al., 2025; Jin et al., 2025b; Hedlin et al., 2023; Tang et al., 2023; Xiao et al., 2024) and DiT-based (Yu et al., 2025; Nam et al., 2025a; Jin et al., 2025a; Lee et al., 2025) models show that query-key matching encodes semantic correspondences. Editing and customization studies (Nam et al., 2024a; Cao et al., 2023; Jin et al., 2025b; Hertz et al., 2022; Tumanyan et al., 2022) consistently report that query-key matching captures structure and semantic alignment, while values carry an appearance that is routed to attended locations. These findings enable strong layout preservation and controllable appearance transfer, and also supports downstream tasks such as tracking (Jeong et al., 2025; Nam et al., 2025a).

Correspondence in VTON. Several VTON works (Wan et al., 2025; Chen et al., 2024; Huang et al., 2022) inject sparse, point-based correspondences into attention or warp features around a few matched points, which provides only local supervision and often breaks under occlusions and large pose variations in unpaired settings. Beyond sparse correspondences, some (Zhou et al., 2024) derives dense flows from attention, but in unpaired settings, such photometric assumption (Truong et al., 2021) fails more often, degrading the performance. Our approach instead operates in DiTs and explicitly strengthens query-key matching by aligning attention to external, robust person-garment correspondences from DINOv3 (Siméoni et al., 2025), reducing reliance on photometric consistency.

3. Preliminaries

Latent Diffusion Models (LDM). LDM (Rombach et al., 2022) operates in latent space, consisting of VAE and denoiser $\epsilon_\theta(\cdot)$. The VAE encoder maps an image $I \in \mathbb{R}^{H \times W \times 3}$ into a latent representation $\mathbf{z}_0 \in \mathbb{R}^{h \times w \times c}$, where $(H, W, 3)$ and (h, w, c) denote the height, width, and channel dimensions in RGB and latent spaces, respectively. At

a timestep t , Gaussian noise $\epsilon \sim \mathcal{N}(0, \mathbf{I})$ is added to \mathbf{z}_0 , producing noisy latent \mathbf{z}_t . Given conditioning tokens \mathbf{c} , we follow rectified flow (Esser et al., 2024), where the model predicts the velocity transporting a clean latent toward Gaussian noise. Specifically, at a timestep t , a linearly interpolated latent is constructed as

$$\mathbf{z}_t = (1 - t) \mathbf{z}_0 + t \epsilon, \quad \epsilon \sim \mathcal{N}(0, \mathbf{I}), \quad (1)$$

and the velocity network $\mathbf{v}_\theta(\mathbf{z}_t, t, \mathbf{c})$ is trained to approximate the target velocity $(\epsilon - \mathbf{z}_0)$ conditioned on \mathbf{c} . The velocity training objective $\mathcal{L}_{\text{velocity}}$ is defined as

$$\mathcal{L}_{\text{velocity}} = \mathbb{E}_{\mathbf{z}_0, \epsilon, t} \left[\|\mathbf{v}_\theta(\mathbf{z}_t, t, \mathbf{c}) - (\epsilon - \mathbf{z}_0)\|_2^2 \right]. \quad (2)$$

Attention in DiTs. Diffusion Transformers (DiTs) (Peebles & Xie, 2023; Esser et al., 2024) consist of multiple layers of 3D full attention that jointly process visual and textual information. The noisy latent tokens \mathbf{z}_t and the conditioning tokens \mathbf{c}_t at time step t are concatenated to form the input sequence. The conditioning tokens are constructed by concatenating tokens from multiple conditions, $\mathbf{c}_t = [c_{t,1} \| \dots \| c_{t,N}]$, where N denotes the number of conditions and $[\cdot \| \cdot]$ denotes token-wise concatenation. Therefore, the final input sequence is $[\mathbf{z}_t \| \mathbf{c}_t]$. At each timestep t and transformer layer l , the concatenated sequence is projected into queries $Q^{t,l}$ and keys $K^{t,l}$:

$$Q^{t,l} = [Q_{\mathbf{z}}^{t,l} \| Q_{\mathbf{c}_1}^{t,l} \| \dots \| Q_{\mathbf{c}_N}^{t,l}], \quad (3)$$

$$K^{t,l} = [K_{\mathbf{z}}^{t,l} \| K_{\mathbf{c}_1}^{t,l} \| \dots \| K_{\mathbf{c}_N}^{t,l}]. \quad (4)$$

Each token in the sequence is augmented with rotary position embeddings (RoPE) (Su et al., 2023). The attention map $A^{t,l}$ at timestep t and layer l is then computed as:

$$A^{t,l} = \text{Softmax} \left(\frac{Q^{t,l} (K^{t,l})^\top}{\sqrt{d}} \right), \quad (5)$$

where $\text{Softmax}(\cdot)$ is applied over the key dimension for each query, and d denotes a channel dimension. To sum up, this full attention determines how each latent or conditioning token attends to every other token in the sequence.

4. Method

4.1. Task Definition

Let $I_p \in \mathbb{R}^{H \times W \times 3}$ denote a person image, $I_g \in \mathbb{R}^{H \times W \times 3}$ a garment image, and $I_{\text{pose}} \in \mathbb{R}^{H \times W \times 3}$ a pose image (estimated from I_p). Let $M_p, M_g \in \mathbb{R}^{H \times W}$ be binary masks indicating garment regions in I_p and I_g , respectively, and $M_e \in \mathbb{R}^{H \times W \times 3}$ be a binary inpainting mask, specifying the region to be edited in I_p , where $M_p \subseteq M_e$. Given the inputs $\{I_p, I_g, I_{\text{pose}}, M_p, M_g, M_e\}$, our goal is to synthesize a try-on image \hat{I} that (i) preserves the appearance of I_p within

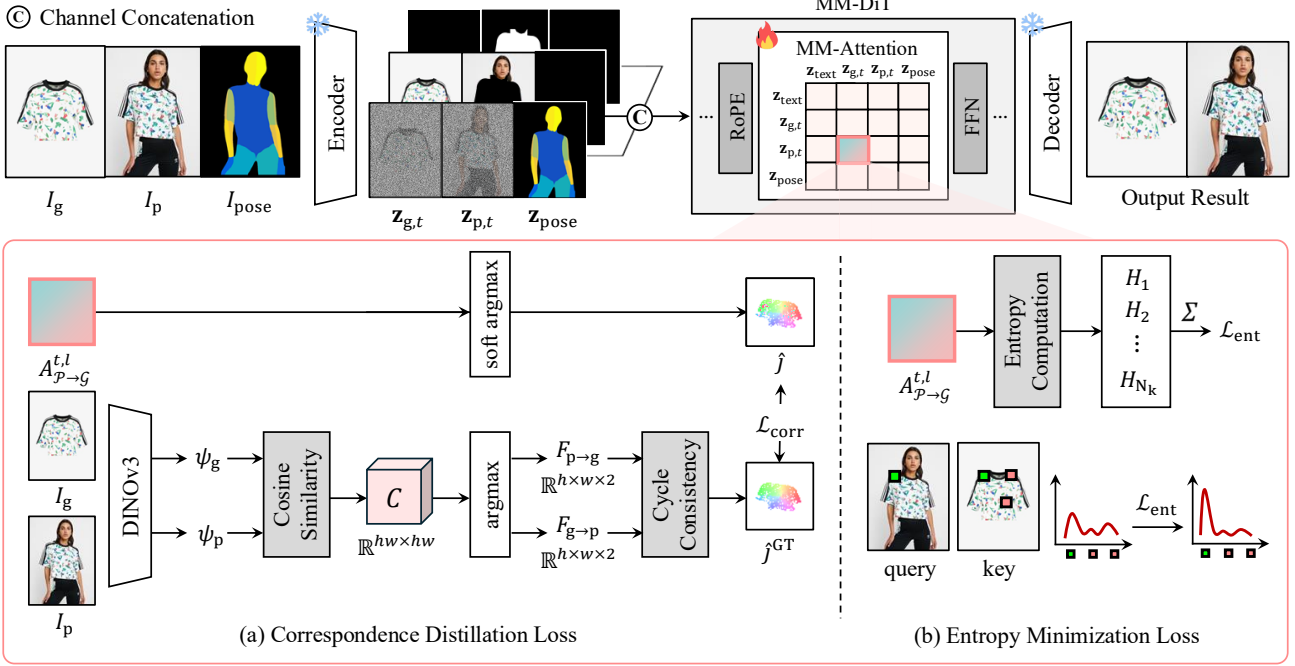


Figure 3. Overall Architecture. CORAL builds upon a baseline architecture that constructs the noisy latent \mathbf{z}_t by horizontally concatenating the noisy garment latents $\mathbf{z}_{g,t}$ and person latents $\mathbf{z}_{p,t}$, and then channel-wise concatenates the conditioning canvas $\mathbf{m}_{\text{diptych}}$ and mask canvas $\mathbf{m}_{\text{diptych}}$ with \mathbf{z}_t before the input projection layer. Pose is injected by adding \mathbf{z}_{pose} as tokens, with RoPE set to share spatial positions between person and pose tokens. $\mathcal{L}_{\text{CORAL}}$ is applied to the person \rightarrow garment matching cost $A_{p \rightarrow g}^{t,l}$ estimated from MM-Attention within DiT blocks: $\mathcal{L}_{\text{corr}}$ aligns $A_{p \rightarrow g}^{t,l}$ to pseudo ground-truth correspondences extracted from DINOv3, while \mathcal{L}_{ent} is computed on $A_{p \rightarrow g}^{t,l}$ to encourage sharper, more localized matches.

the region specified by M_e , (ii) follows the pose defined by I_{pose} , and (iii) accurately transfers the shape and local details of the garment I_g according to M_g into the person image, restricted to M_e .

4.2. Network Architecture

Diptych Formulation. We first build a DiT-based baseline with a simple conditioning design, leveraging DiT’s in-context conditioning ability for reference-guided generation (Shin et al., 2025; Huang et al., 2024). We adopt a two-panel diptych layout that horizontally concatenates garment and person latents to enable direct token-level interaction through multimodal attention, instead of relying on auxiliary encoders to integrate garment. The overall architecture is illustrated in Fig. 3.

Specifically, we encode the garment and person images, I_g and I_p , with a VAE to obtain \mathbf{z}_g and \mathbf{z}_p , and form a two-panel latent canvas. At timestep t , we construct the noisy diptych latent as:

$$\mathbf{z}_t = [\mathbf{z}_{g,t} \parallel \mathbf{z}_{p,t}], \quad (6)$$

where $\mathbf{z}_{g,t}$ and $\mathbf{z}_{p,t}$ are noisy garment and person latents at timestep t . For conditioning clean garment and masked person image, we use the clean garment latent and the masked

person latent as:

$$\mathbf{z}_{\text{diptych}} = [\mathbf{z}_g \parallel \mathbf{z}_p \odot (1 - \mathbf{m}_e)], \quad (7)$$

where \mathbf{m}_e is obtained by downsampling M_e into the latent space. We also define a binary mask canvas $\mathbf{m}_{\text{diptych}}$ following the same two-panel layout, assigning ones to the region to be replaced and zeros elsewhere:

$$\mathbf{m}_{\text{diptych}} = [\mathbf{0}_{h \times w} \parallel \mathbf{m}_e]. \quad (8)$$

Pose Injection. Previous try-on methods often suffer from pose hallucination and hand inconsistencies, where the synthesized results fail to align with the input pose and distort hand shapes. To mitigate this, a common design in prior methods is to concatenate a pose condition \mathbf{z}_{pose} , obtained by encoding I_{pose} with a VAE, with the noisy person latent $\mathbf{z}_{p,t}$ along the channel dimension (Choi et al., 2024; Kim et al., 2023). However, we find this approach suboptimal for strict pose alignment, as the person appearance and pose conditions become entangled in the latent space.

Inspired by recent DiT-based conditioning framework (Tan et al., 2025a), our main baseline instead concatenates clean pose condition \mathbf{z}_{pose} along the token dimension, forming $[\mathbf{z}_{g,t} \parallel \mathbf{z}_{p,t} \parallel \mathbf{z}_{\text{pose}}]$ as input. We then enforce spatial alignment by modifying RoPE (Su et al., 2023) so that $\mathbf{z}_{p,t}$ and \mathbf{z}_{pose} share the same positional indices, which provides strong

positional correspondence and allows pose to be integrated more coherently through full attention over the joint sequence. To match the input channel dimension, we zero pad $\mathbf{z}_{\text{diptych}}$, and $\mathbf{m}_{\text{diptych}}$. Finally, zero-padded $\mathbf{z}_{\text{diptych}}$ and $\mathbf{m}_{\text{diptych}}$ are channel-wise concatenated with $[\mathbf{z}_t \parallel \mathbf{z}_{\text{pose}}]$ as the input for the embedding layer, and the resulting tokens are then passed to the DiT.

4.3. Person-Garment Correspondence Analysis

Motivation. A major challenge in VTON is establishing accurate correspondence between the person and the garment to reliably transfer local garment details and shape onto the person image. One approach may be to align DiT intermediate features with strong matching descriptors (e.g., DINOv3 (Siméoni et al., 2025)), but this often disrupts the model’s learned generative representations and requires full retraining (Yu et al., 2025). An alternative is to distill reliable correspondence into DiT intermediate features, however, as discussed in prior works (An et al., 2025; Nam et al., 2024a), these features contain appearance information from value matrices that weakens spatial relationships, making them suboptimal for precise matching. Additional explorations are provided in Appendix E.

To address these limitations, we leverage query–key attention within the DiT’s full 3D attention, which implicitly models interactions between person and garment tokens (Nam et al., 2025a) without disrupting appearances.

Correspondence Estimation. To examine how spatial alignment between garment and person features is established in the baseline DiTs, we extract query–key correspondences from the DiTs attention. Following Eq. 4, the query and key at timestep t and layer l are composed of:

$$Q^{t,l} = [Q_{\mathbf{z}_{\text{text}}}^{t,l} \parallel Q_{\mathbf{z}_g}^{t,l} \parallel Q_{\mathbf{z}_p}^{t,l} \parallel Q_{\mathbf{z}_{\text{pose}}}^{t,l}], \quad (9)$$

$$K^{t,l} = [K_{\mathbf{z}_{\text{text}}}^{t,l} \parallel K_{\mathbf{z}_g}^{t,l} \parallel K_{\mathbf{z}_p}^{t,l} \parallel K_{\mathbf{z}_{\text{pose}}}^{t,l}]. \quad (10)$$

Here, $Q_{\mathbf{z}_{\text{text}}}^{t,l}$ and $K_{\mathbf{z}_{\text{text}}}^{t,l}$ correspond to the input text tokens. We define m_p and m_g as the downsampled versions of M_p and M_g . Let \mathcal{P} and \mathcal{G} be the index sets of person and garment tokens whose spatial locations fall inside m_p and m_g , respectively, corresponding to the masked subsets of $Q_{\mathbf{z}_p}^{t,l}$ and $K_{\mathbf{z}_g}^{t,l}$. Using Eq. 5, we compute the person→garment attention with $Q_{\mathbf{z}_p}^{t,l}$ as queries and $K_{\mathbf{z}_g}^{t,l}$ as keys, resulting in:

$$A_{\mathcal{P} \rightarrow \mathcal{G}}^{t,l} := A^{t,l}[\mathcal{P}, \mathcal{G}] \in \mathbb{R}^{|\mathcal{P}| \times |\mathcal{G}|}. \quad (11)$$

We treat $A_{\mathcal{P} \rightarrow \mathcal{G}}^{t,l}$ as the matching cost between the person and garment latents. This aligns with analyses in (Nam et al., 2024a; 2025a), but no prior work frames the VTON task as person–garment correspondence within DiT attention. For simplicity, the variables t and l are omitted from the following equations.

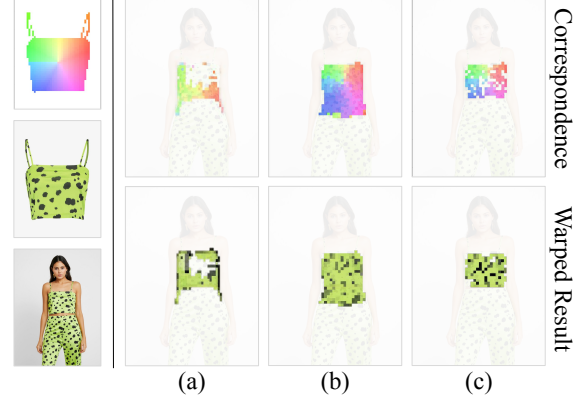


Figure 4. Correspondence Visualization and Warped Results. We visualize correspondence fields and the resulting warped garment, computed by mapping pixels from the garment reference image to the garment region of the person image. (a) Baseline attention-derived correspondence. (b) DINOv3 correspondence before reliability filtering. (c) Refined correspondence after cycle-consistency check. The baseline warp shows geometric distortion, while unfiltered DINOv3 can mistakenly match visually similar regions, such as lower-garment areas.

From these matching costs, we extract dense correspondences from person spatial location i to garment latents by taking $\arg \max$ over garment tokens:

$$\hat{j}_i = \arg \max_{j \in \mathcal{G}} A_{\mathcal{P} \rightarrow \mathcal{G}}(i, j). \quad (12)$$

Evaluation Benchmark. To validate query–key correspondence in the baseline architecture, we require ground-truth person–garment correspondences. Since such annotations do not exist, we construct pseudo ground-truth matches using DINOv3 (Siméoni et al., 2025), a vision foundation model, shown to be highly effective for dense matching. Given I_p and I_g , we extract feature descriptors $\phi(\cdot)$ from DINOv3 and keep only tokens inside the downsampled masks:

$$\psi_p = \phi(I_p) \odot m_p, \quad \psi_g = \phi(I_g) \odot m_g. \quad (13)$$

Following standard dense matching protocols (Hong et al., 2022a;b; Cho et al., 2024; Nam et al., 2024b), we compute the matching cost between descriptors using cosine similarity:

$$C(i, j) = \frac{\psi_p(i) \cdot \psi_g(j)}{\|\psi_p(i)\|_2 \|\psi_g(j)\|_2}, \quad (14)$$

where i and j index the spatial locations of the person and garment descriptors, respectively.

To obtain reliable pseudo ground-truth matches, we introduce a reliability mask $\mathbf{m}_{\text{rel}}(i)$ that filters out unstable correspondences using a cycle-consistency (Jiang et al., 2021) constraint. We first estimate bidirectional flow, which are person to garment, $F_{p \rightarrow g} \in \mathbb{R}^{h \times w \times 2}$, and garment to person, $F_{g \rightarrow p} \in \mathbb{R}^{h \times w \times 2}$, by taking the $\arg \max$ over spatial

locations of garment and person in the matching cost, respectively. The reliability mask identifies points whose matched locations in the garment features return to the original locations in the person features within a specified threshold γ :

$$\mathbf{m}_{\text{rel}}(i) = \begin{cases} 1, & \text{if } \|F_{g \rightarrow p}(F_{p \rightarrow g}(i)) - i\|_2 < \gamma, \\ 0, & \text{otherwise.} \end{cases} \quad (15)$$

Finally, we obtain pseudo ground-truth correspondences by applying the reliability mask to the garment points corresponding to each location, as illustrated in Fig. 4 (c):

$$\hat{j}_i^{\text{GT}} = \mathbf{m}_{\text{rel}}(i) \cdot \arg \max_{j \in \Omega} C(i, j), \quad (16)$$

where Ω is the garment spatial domain.

Query-Key Matching and Performance. By comparing attention-derived correspondences with the pseudo-ground truth from DINOv3, we observe a correlation between matching accuracy and the quality of the try-on results. As shown in Fig. 2, cases with accurate RGB alignment between the person and garment exhibit sharp, well-localized query-key attention, while suboptimal cases with artifacts on garments show dispersed or misplaced attention.

To quantify this observation, we sample 540 pairs from the VITON-HD (Choi et al., 2021) test set and evaluate point accuracy using Percentage of Correct Keypoints (PCK), which measures the proportion of predictions within distance α of the ground-truth correspondence (Eq. 17), formulated as:

$$\text{PCK}(\alpha) = \frac{1}{N} \sum_{i=1}^N \mathbf{1}[\|\hat{j}_i - \hat{j}_i^{\text{GT}}\|_2 < \alpha], \quad (17)$$

where $\mathbf{1}(\cdot)$ is an indicator function, N is the number of evaluated correspondences, determined by the garment region \mathbf{m}_p and the reliability mask \mathbf{m}_{rel} , and α is a distance threshold. VTON performance is assessed using SSIM (Cong et al., 2022) and LPIPS (Zhang et al., 2018).

As shown in Fig. 2 (b), PCK exhibits a positive correlation with SSIM and a negative correlation with LPIPS, indicating that higher query-key matching accuracy leads to better structural fidelity and perceptual quality in the try-on results. These findings highlight the importance of accurate query-key matching for VTON and motivate us to explicitly guide the attention toward stronger correspondence.

4.4. CORAL: Correspondence Alignment

Based on our analysis, we introduce CORAL, which integrates reliable DINOv3-derived matches into the baseline’s query-key matching for robust virtual try-on performance.

Correspondence Distillation Loss. We aim to align the estimated matches obtained from query-key attention

with the pseudo ground-truth matches provided by DINOv3 (Siméoni et al., 2025). Because the argmax operation is not differentiable (Eq. 12), we use a soft argmax to predict the estimated correspondences from the query-key attention, formulated as follows:

$$\hat{j}_i = \sum_{j=1}^N A_{p \rightarrow g}(i, j) \cdot j. \quad (18)$$

Finally, we compute the mean L2 loss between estimated correspondences and the pseudo ground-truth matches:

$$\mathcal{L}_{\text{corr}} = \frac{1}{N} \sum_{i=1}^N \|\hat{j}_i - \hat{j}_i^{\text{GT}}\|_2^2. \quad (19)$$

Entropy Minimization Loss. The correspondence distillation loss ($\mathcal{L}_{\text{corr}}$) aligns query-key matches with external pseudo-matches. However, this alignment is unreliable when the attention distribution becomes overly diffuse, as incorrect key positions can then dominate the weighted average. To ensure robust correspondence supervision, we introduce an entropy minimization loss that promotes confident, spatially localized query-key alignments.

To implement this, we define the entropy based on the attention distribution. Following Shannon’s definition of entropy (Attanasio et al., 2022), we compute the entropy H_i for a given query i by treating its attention weights $A(i, \cdot)$ over the keys as a probability distribution, formulated as:

$$H_i = - \sum_{j=1}^{N_k} A(i, j) \log A(i, j), \quad (20)$$

where N_k is the total number of key tokens. Averaging H_i over all N query tokens yields the entropy minimization loss:

$$\mathcal{L}_{\text{ent}} = \frac{1}{N} \sum_{i=1}^N H_i. \quad (21)$$

Lower entropy corresponds to sharper and more confident attention, whereas higher entropy indicates diffuse or uncertain matching. Entropy minimization loss (\mathcal{L}_{ent}) therefore complements the correspondence distillation loss ($\mathcal{L}_{\text{corr}}$) by enforcing sharper, and more reliable alignments.

Total Loss. Finally, we define CORAL loss as a weighted combination of the correspondence and entropy terms:

$$\mathcal{L}_{\text{CORAL}} = \lambda_{\text{corr}} \mathcal{L}_{\text{corr}} + \lambda_{\text{ent}} \mathcal{L}_{\text{ent}}, \quad (22)$$

where λ_{corr} and λ_{ent} are empirically set.

We then optimize the final objective by adding CORAL loss:

$$\mathcal{L}_{\text{total}} = \mathcal{L}_{\text{velocity}} + \mathcal{L}_{\text{CORAL}}. \quad (23)$$

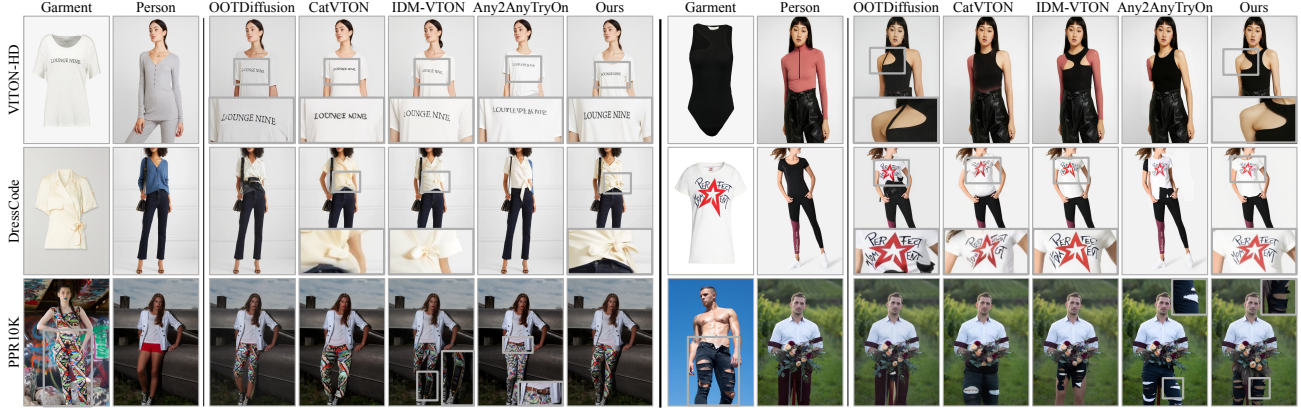


Figure 5. **Qualitative Comparison.** We show qualitative results on the standard benchmarks VITON-HD (Choi et al., 2021) and DressCode (Morelli et al., 2022), as well as in-the-wild evaluation dataset built from PPR10K (Liang et al., 2021) (Best viewed when zoomed-in). Additional qualitative results are provided in Appendix J

Table 1. Quantitative Comparison on VITON-HD (Choi et al., 2021).

Methods	Paired			Unpaired		
	SSIM \uparrow	LPIPS \downarrow	FID \downarrow	KID \downarrow	FID \downarrow	KID \downarrow
GPVTON (Xie et al., 2023)	0.878	0.067	8.938	4.257	11.993	4.570
StableVTION (Kim et al., 2023)	0.888	0.073	8.233	0.490	9.026	3.029
OOTDiffusion (Kim et al., 2023)	0.842	0.087	6.619	0.845	9.938	1.302
IDM-VTON (Choi et al., 2024)	0.866	0.062	6.009	0.838	9.198	1.203
CatVTON (Chong et al., 2025)	0.874	0.058	5.458	0.439	9.076	1.184
Any2AnyTryOn (Guo et al., 2025)	0.838	0.087	5.482	0.384	9.623	1.601
CORAL (w/o $\mathcal{L}_{\text{CORAL}}$)	0.889	0.055	5.543	0.870	9.641	1.323
CORAL (w $\mathcal{L}_{\text{CORAL}}$)	0.907	0.048	4.962	0.565	8.763	0.880

Table 2. Quantitative Comparison on DressCode (Morelli et al., 2022).* does not support paired setting on specific dataset.

Methods	Paired			Unpaired		
	SSIM \uparrow	LPIPS \downarrow	FID \downarrow	KID \downarrow	FID \downarrow	KID \downarrow
GPVTON (Xie et al., 2023)	0.918	0.068	8.423	2.439	9.144	3.936
OOTDiffusion (Xu et al., 2024)	0.880	0.069	5.082	1.377	9.276	4.009
IDM-VTON (Choi et al., 2024)	0.904	0.052	3.472	0.882	5.343	1.321
CatVTON (Chong et al., 2025)	0.875	0.075	5.384	1.903	7.998	3.242
Any2AnyTryOn* (Guo et al., 2025)	-	-	-	-	5.573	1.458
CORAL (w/o $\mathcal{L}_{\text{CORAL}}$)	0.908	0.045	2.896	0.418	5.221	1.315
CORAL (w $\mathcal{L}_{\text{CORAL}}$)	0.927	0.029	2.333	0.401	4.692	0.846

5. Experiments

5.1. Evaluation Setting

Evaluation Dataset. We train separate models on the standard VTON datasets, **VITON-HD** (Han et al., 2018) and **DressCode** (Morelli et al., 2022), both at a resolution of 1024×768 , and evaluate them on their respective test sets. More implementation details are provided in Appendix A.

In addition to standard VTON benchmarks, we further evaluate zero-shot generalization on the **PPR10K** (Liang et al., 2021), which provides less curated inputs than the in-shop product image setting. For this evaluation, we use a pre-trained checkpoint trained on DressCode. We also include the worn-garment setting, where the reference garment is shown on another person. Additional details on PPR10K evaluation are provided in Appendix H.

Metrics. We report conventional metrics SSIM (Cong et al., 2022), LPIPS (Zhang et al., 2018), FID (Heusel et al., 2018)

Table 3. Quantitative Comparison on PPR10K (Liang et al., 2021).* does not support paired setting on specific dataset.

Methods	Paired			Unpaired		
	SSIM \uparrow	LPIPS \downarrow	FID \downarrow	KID \downarrow	FID \downarrow	KID \downarrow
OOTDiffusion (Kim et al., 2023)	0.804	0.130	99.492	15.592	87.818	15.467
IDM-VTON (Choi et al., 2024)	0.844	0.111	64.250	1.911	63.638	3.600
CatVTON (Chong et al., 2025)	0.743	0.147	81.722	10.979	76.417	11.207
Any2AnyTryOn* (Guo et al., 2025)	-	-	-	-	49.728	0.421
CORAL (w/o $\mathcal{L}_{\text{CORAL}}$)	0.877	0.078	44.117	0.015	56.644	1.202
CORAL (w $\mathcal{L}_{\text{CORAL}}$)	0.915	0.060	43.648	0.011	53.164	1.101

Table 4. VLM-based evaluation on unpaired settings.* does not support inference on specific dataset.

Train/Test	VITON-HD/VITON-HD			DressCode/DressCode			DressCode/PPR10K		
	GTC \uparrow	TAC \uparrow	FPC \uparrow	GTC \uparrow	TAC \uparrow	FPC \uparrow	GTC \uparrow	TAC \uparrow	FPC \uparrow
GPVTON* (Xie et al., 2023)	3.93	4.28	4.17	3.19	3.31	3.14	-	-	-
OOTDiffusion (Xu et al., 2024)	3.97	4.34	4.12	3.25	3.24	3.45	1.04	2.06	1.57
IDM-VTON (Choi et al., 2024)	3.96	4.40	4.25	3.25	3.28	3.61	1.72	2.21	2.37
CatVTON (Chong et al., 2025)	3.82	4.20	4.06	3.07	3.22	3.53	1.05	2.00	2.01
Any2AnyTryOn* (Guo et al., 2025)	3.81	4.27	4.19	2.99	3.28	3.36	1.92	2.45	2.48
CORAL (Ours)	3.99	4.40	4.26	3.47	3.31	3.83	2.07	2.56	2.89

and KID (Bińkowski et al., 2021) for paired settings, and measure FID and KID for unpaired settings.

VLM-based Evaluation. As discussed in prior studies (Xi-aobin et al., 2025), existing metrics such as FID and KID are insufficient to reflect human preference especially in the unpaired setting. Such distribution based metrics primarily measure overall realism, but do not verify whether the specific garment in the reference has been faithfully transferred and plausibly worn. We therefore evaluate three aspects that existing metrics inadequately reflect: **(1) Garment Transfer Consistency (GTC)** measures whether the output preserves the garment’s visual appearance, including its overall shape and silhouette as well as details like patterns, logos, and texture. **(2) Textual Attribute Consistency (TAC)** captures whether the output satisfies garment attributes specified in text or metadata, covering requirements that may be ambiguous from the reference image alone (e.g., length, neckline, category, and fit). **(3) Fit Pose Coherence (FPC)** reflects whether the garment is worn naturally on the target person, consistent with the input person pose and body geometry. It also considers whether non-target regions (e.g., hair, skin, hands, and other clothing) are preserved without unintended changes. Additional details in

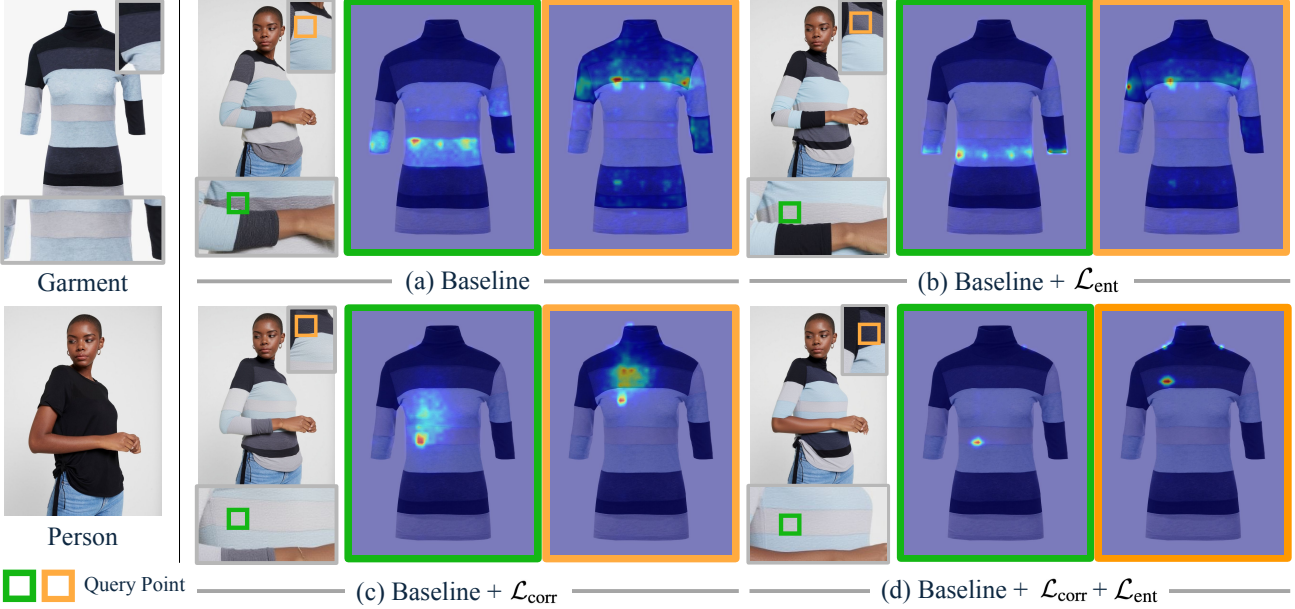


Figure 6. Ablation of Loss Components. We demonstrate the effectiveness of the two losses, \mathcal{L}_{ent} and $\mathcal{L}_{\text{corr}}$. Orange and green markers denote query points, and attention maps outlined in the same colors indicate the matches for each variant. By combining \mathcal{L}_{ent} with $\mathcal{L}_{\text{corr}}$, our model localizes the correct keys most accurately and exhibits the sharpest attention, yielding the best VTON performance.

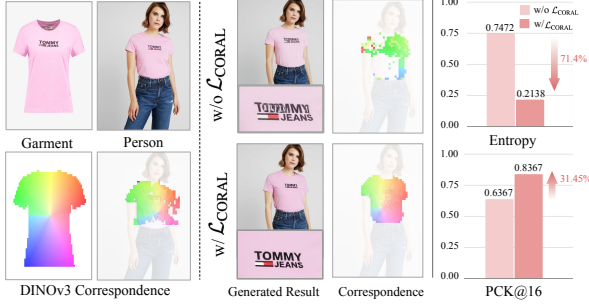


Figure 7. Effect of $\mathcal{L}_{\text{CORAL}}$. We visualize person→garment correspondences from DiT attention and the resulting try-on images before and after applying $\mathcal{L}_{\text{CORAL}}$. The rightmost plot shows correspondence quality measured by PCK ($\alpha = 16$) and attention entropy, averaged across timesteps and layers.

the Appendix F and G support the reliability of our protocol.

5.2. Quantitative Comparison

Main Results. Tab. 1 and Tab. 2 report quantitative comparisons on VITON-HD (Choi et al., 2021) and Dress-Code (Morelli et al., 2022). CORAL achieves the best overall performance on both benchmarks. Tab. 3 further shows that CORAL achieves the best results in the paired setting across all metrics, and remains competitive in the unpaired setting while substantially outperforming the other baselines on the additional in-the-wild dataset. Across all three tables, our baseline (w/o $\mathcal{L}_{\text{CORAL}}$) is already strong, but adding CORAL consistently improves every metric, indicating reliable gains beyond a competitive baseline and robust improvements in perceptual fidelity, even in the in-the-wild setting.

Table 5. Ablation of Loss Components on VITON-HD.

	$\mathcal{L}_{\text{corr}}$	\mathcal{L}_{ent}	Paired				Unpaired	
			SSIM \uparrow	LPIPS \downarrow	FID \downarrow	KID \downarrow	FID \downarrow	KID \downarrow
(I)	✗	✗	0.889	0.055	5.543	0.870	9.641	1.423
(II)	✗	✓	0.905	0.052	5.482	0.986	9.012	1.011
(III)	✓	✗	0.906	0.051	5.451	1.028	8.979	1.250
(IV)	✓	✓	0.907	0.048	4.962	0.565	8.763	0.880

VLM Evaluation Results. Tab. 4 presents quantitative results of VLM-based evaluation. Compared to prior methods, CORAL achieves the best performance across all three metrics. By determining query-key matches at the correct person-garment locations, CORAL transfers appearance from the correct regions, which improves GTC. More accurate spatial correspondences also better preserve garment attributes such as silhouette and length, pattern geometry, increasing TAC. These gains produce more natural wear and pose following, reflected in the highest FPC.

5.3. Qualitative Comparison

Fig. 5 shows qualitative comparisons between previous works and CORAL. CORAL preserves global garment properties, while recovering fine local details (e.g., logos) that the baseline often misses. We also observe that CORAL keeps garment text clear and readable, while other methods often blur, deform, or remove it. In addition, some baselines deviate from the input pose with subtle pose shifts, while CORAL keeps the pose closer to the input. The improvement comes from correcting person-garment matches in DiT attention, thereby transferring appearance from the correct locations. Additional qualitative comparisons with previous works and baseline are provided in Appendix J.

5.4. Ablation Study

Ablation of Loss Components. Fig. 6 and Tab. 5 highlight the effects of our loss design. (a) and (I) show the baseline, where attention is poorly localized and often dispersed away from query-relevant regions, yielding misaligned correspondences and artifacts. Pattern placement is frequently incorrect in (a), and (I) shows the weakest performance. (b) and (II) present the effect of \mathcal{L}_{ent} , which sharpens attention and improves fine detail transfer (e.g., colors, textures). However, \mathcal{L}_{ent} does not correct *where* the model matches, so the coarse garment properties such as length, often remain inaccurate. Moreover, when sharpening occurs on wrong matches, the model often transfer inappropriate appearance. This explains why (II) improves perceptual and reconstruction metrics (SSIM, LPIPS) over (I), while still exhibiting misalignment in challenging cases. (c) and (III) show the effect of $\mathcal{L}_{\text{corr}}$, which relocates correspondences to the correct garment regions and improves coarse properties (e.g., silhouette, pattern geometry). Nevertheless, attention remains relatively diffuse, which limits the accurate transfer of fine details when the matched key has low attention mass. Compared to (b), (c) has a more accurate geometry, but lag behind in appearance richness such as color fidelity. (d) and (IV) present the combination of \mathcal{L}_{ent} and $\mathcal{L}_{\text{corr}}$, which integrates these complementary gains. This yields both accurate alignment and sharp detail transfer, leading to the best qualitative results and the strongest quantitative performance across all metrics.

Analysis of CORAL on Attention Correspondence. Fig. 7 summarizes how $\mathcal{L}_{\text{CORAL}}$ affects person→garment attention $A^{t,l}[\mathcal{P}, \mathcal{G}]$ and generated results. Without $\mathcal{L}_{\text{CORAL}}$, the correspondence maps still contain noticeable mismatches near local textures and garment boundaries, even when the overall vertical alignment appears plausible. These mismatches cause the logo patterns not to appear clearly in the generated result. Adding $\mathcal{L}_{\text{CORAL}}$ consistently corrects the correspondence maps, producing matches that more closely follow the DINOv3 pseudo ground-truth matches in Fig. 7, leading to improved text details, with correctly generated letters. Fig. 7 also shows this quantitatively: $\mathcal{L}_{\text{CORAL}}$ improves PCK by 34 % while reducing attention entropy, indicating more accurate and sharper correspondences in attention.

6. Conclusion

We analyze how person→garment correspondence is established within the full 3D attention of DiT for VTON and show that RGB-space person–garment alignment depends on accurate query–key correspondence. We introduce CORAL, a DiT-based framework that aligns person–garment query–key matches with robust DINOv3 correspondences. CORAL incorporates a correspondence distillation loss to align robust matches with attention, along

with an entropy minimization loss to sharpen attention. As a result, CORAL achieves state-of-the-art performance across all standard benchmarks as well as an in-the-wild benchmark. Extensive analyses and ablation studies further demonstrate the effectiveness of our design choices.

Acknowledgements

This work was partly supported by the Institute of Information & Communications Technology Planning & Evaluation (IITP) grant funded by the Korea government (MSIT) (No. RS-2025-25441313, Professional AI Talent Development Program for Multimodal AI Agents, Contribution: 50%).

Impact Statement

This paper presents work whose goal is to advance the field of machine learning. There are many potential societal consequences of our work, none of which we feel must be specifically highlighted here.

References

An, H., Kim, J. H., Park, S., Jung, J., Han, J., Hong, S., and Kim, S. Cross-view completion models are zero-shot correspondence estimators. In *Proceedings of the Computer Vision and Pattern Recognition Conference*, pp. 1103–1115, 2025. 5

Attanasio, G., Nozza, D., Hovy, D., and Baralis, E. Entropy-based attention regularization frees unintended bias mitigation from lists, 2022. URL <https://arxiv.org/abs/2203.09192>. 6

Bhunia, A. K., Khan, S., Cholakkal, H., Anwer, R. M., Laaksonen, J., Shah, M., and Khan, F. S. Person image synthesis via denoising diffusion model, 2023. URL <https://arxiv.org/abs/2211.12500>. 2, 3

Bińkowski, M., Sutherland, D. J., Arbel, M., and Gretton, A. Demystifying mmd gans, 2021. URL <https://arxiv.org/abs/1801.01401>. 7, 19

Cao, M., Wang, X., Qi, Z., Shan, Y., Qie, X., and Zheng, Y. Masactrl: Tuning-free mutual self-attention control for consistent image synthesis and editing, 2023. URL <https://arxiv.org/abs/2304.08465>. 3

Cao, Z., Hidalgo, G., Simon, T., Wei, S.-E., and Sheikh, Y. Openpose: Realtime multi-person 2d pose estimation using part affinity fields. *IEEE Transactions on Pattern Analysis and Machine Intelligence*, 43(1):172–186, 2021. doi: 10.1109/TPAMI.2019.2929257. 22, 23

Carion, N., Gustafson, L., Hu, Y.-T., Debnath, S., Hu, R., Suris, D., Ryali, C., Alwala, K. V., Khedr, H., Huang,

A., Lei, J., Ma, T., Guo, B., Kalla, A., Marks, M., Greer, J., Wang, M., Sun, P., Rädle, R., Afouras, T., Mavroudi, E., Xu, K., Wu, T.-H., Zhou, Y., Momeni, L., Hazra, R., Ding, S., Vaze, S., Porcher, F., Li, F., Li, S., Kamath, A., Cheng, H. K., Dollár, P., Ravi, N., Saenko, K., Zhang, P., and Feichtenhofer, C. Sam 3: Segment anything with concepts, 2025. URL <https://arxiv.org/abs/2511.16719>. 14, 23

Chen, M., Chen, X., Zhai, Z., Ju, C., Hong, X., Lan, J., and Xiao, S. Wear-any-way: Manipulable virtual try-on via sparse correspondence alignment, 2024. URL <https://arxiv.org/abs/2403.12965>. 3, 18

Chen, Q., Qin, L., Liu, J., Peng, D., Guan, J., Wang, P., Hu, M., Zhou, Y., Gao, T., and Che, W. Towards reasoning era: A survey of long chain-of-thought for reasoning large language models, 2025. URL <https://arxiv.org/abs/2503.09567>. 19

Cheng, Z., Xu, B., Gong, L., Song, Z., Zhou, T., Zhong, S., Ren, S., Chen, M., Meng, X., Zhang, Y., Li, Y., Ren, L., Chen, W., Huang, Z., Zhan, M., Wang, X., and Feng, F. Evaluating mllms with multimodal multi-image reasoning benchmark, 2025. URL <https://arxiv.org/abs/2506.04280>. 19

Cho, S., Huang, J., Nam, J., An, H., Kim, S., and Lee, J.-Y. Local all-pair correspondence for point tracking. In *European conference on computer vision*, pp. 306–325. Springer, 2024. 5

Choi, S., Park, S., Lee, M., and Choo, J. Viton-hd: High-resolution virtual try-on via misalignment-aware normalization, 2021. URL <https://arxiv.org/abs/2103.16874>. 6, 7, 8, 14, 15, 16, 17, 25, 28

Choi, Y., Kwak, S., Lee, K., Choi, H., and Shin, J. Improving diffusion models for authentic virtual try-on in the wild, 2024. URL <https://arxiv.org/abs/2403.05139>. 2, 3, 4, 7, 14, 20, 22

Chong, Z., Dong, X., Li, H., Zhang, S., Zhang, W., Zhang, X., Zhao, H., Jiang, D., and Liang, X. Catvton: Concatenation is all you need for virtual try-on with diffusion models, 2025. URL <https://arxiv.org/abs/2407.15886>. 2, 3, 7, 14, 20

Cong, H., Fu, L., Zhang, R., Zhang, Y., Wang, H., He, J., and Gao, J. Image quality assessment with gradient siamese network, 2022. URL <https://arxiv.org/abs/2208.04081>. 6, 7, 19

Dai, W., Li, J., Li, D., Tiong, A. M. H., Zhao, J., Wang, W., Li, B., Fung, P., and Hoi, S. Instructblip: Towards general-purpose vision-language models with instruction tuning, 2023. URL <https://arxiv.org/abs/2305.06500>. 19

Esser, P., Kulal, S., Blattmann, A., Entezari, R., Müller, J., Saini, H., Levi, Y., Lorenz, D., Sauer, A., Boesel, F., Podell, D., Dockhorn, T., English, Z., Lacey, K., Goodwin, A., Marek, Y., and Rombach, R. Scaling rectified flow transformers for high-resolution image synthesis, 2024. URL <https://arxiv.org/abs/2403.03206>. 2, 3

Guo, H., Zeng, B., Song, Y., Zhang, W., Zhang, C., and Liu, J. Any2anytryon: Leveraging adaptive position embeddings for versatile virtual clothing tasks, 2025. URL <https://arxiv.org/abs/2501.15891>. 7, 20

Güler, R. A., Neverova, N., and Kokkinos, I. Densepose: Dense human pose estimation in the wild, 2018. URL <https://arxiv.org/abs/1802.00434>. 14, 22, 23

Han, X., Wu, Z., Wu, Z., Yu, R., and Davis, L. S. Viton: An image-based virtual try-on network, 2018. URL <https://arxiv.org/abs/1711.08447>. 7

Hedlin, E., Sharma, G., Mahajan, S., Isack, H., Kar, A., Tagliasacchi, A., and Yi, K. M. Unsupervised semantic correspondence using stable diffusion, 2023. URL <https://arxiv.org/abs/2305.15581>. 3

Hertz, A., Mokady, R., Tenenbaum, J., Aberman, K., Pritch, Y., and Cohen-Or, D. Prompt-to-prompt image editing with cross attention control, 2022. URL <https://arxiv.org/abs/2208.01626>. 3

Heusel, M., Ramsauer, H., Unterthiner, T., Nessler, B., and Hochreiter, S. Gans trained by a two time-scale update rule converge to a local nash equilibrium, 2018. URL <https://arxiv.org/abs/1706.08500>. 7

Hong, S., Cho, S., Nam, J., Lin, S., and Kim, S. Cost aggregation with 4d convolutional swin transformer for few-shot segmentation. In *European Conference on Computer Vision*, pp. 108–126. Springer, 2022a. 5

Hong, S., Nam, J., Cho, S., Hong, S., Jeon, S., Min, D., and Kim, S. Neural matching fields: Implicit representation of matching fields for visual correspondence. *Advances in Neural Information Processing Systems*, 35:13512–13526, 2022b. 5

Hu, E. J., Shen, Y., Wallis, P., Allen-Zhu, Z., Li, Y., Wang, S., Wang, L., and Chen, W. Lora: Low-rank adaptation of large language models, 2021. URL <https://arxiv.org/abs/2106.09685>. 16

Huang, L., Wang, W., Wu, Z.-F., Shi, Y., Dou, H., Liang, C., Feng, Y., Liu, Y., and Zhou, J. In-context lora for diffusion transformers, 2024. URL <https://arxiv.org/abs/2410.23775>. 4, 14

Huang, Z., Li, H., Xie, Z., Kampffmeyer, M., Cai, Q., and Liang, X. Towards hard-pose virtual try-on via 3d-aware global correspondence learning, 2022. URL <https://arxiv.org/abs/2211.14052>. 3, 18

Jeong, H., Huang, C.-H. P., Ye, J. C., Mitra, N., and Ceylan, D. Track4gen: Teaching video diffusion models to track points improves video generation, 2025. URL <https://arxiv.org/abs/2412.06016>. 3

Jia, B., Zhang, J., Zhang, H., and Wan, X. Exploring and evaluating multimodal knowledge reasoning consistency of multimodal large language models, 2025. URL <https://arxiv.org/abs/2503.04801>. 19

Jiang, W., Trulls, E., Hosang, J., Tagliasacchi, A., and Yi, K. M. Cotr: Correspondence transformer for matching across images, 2021. URL <https://arxiv.org/abs/2103.14167>. 5

Jin, S., Kim, S., Chung, D., Lee, J., Choi, H., Nam, J., Kim, J., and Kim, S. Matrix: Mask track alignment for interaction-aware video generation, 2025a. URL <https://arxiv.org/abs/2510.07310>. 3

Jin, S., Nam, J., Kim, J., Chung, D., Kim, Y.-S., Park, J., Chu, H., and Kim, S. Appearance matching adapter for exemplar-based semantic image synthesis in-the-wild, 2025b. URL <https://arxiv.org/abs/2412.03150>. 3

Kim, J., Gu, G., Park, M., Park, S., and Choo, J. Stableviton: Learning semantic correspondence with latent diffusion model for virtual try-on, 2023. URL <https://arxiv.org/abs/2312.01725>. 2, 3, 4, 7

Kim, J., Jin, H., Park, S., and Choo, J. Promptdresser: Improving the quality and controllability of virtual try-on via generative textual prompt and prompt-aware mask, 2025. URL <https://arxiv.org/abs/2412.16978>. 2, 3

Lee, J.-Y., Cha, B., Kim, J., and Ye, J. C. Aligning text to image in diffusion models is easier than you think, 2025. URL <https://arxiv.org/abs/2503.08250>. 3

Li, F., Zhang, R., Zhang, H., Zhang, Y., Li, B., Li, W., Ma, Z., and Li, C. Llava-next-interleave: Tackling multi-image, video, and 3d in large multimodal models, 2024. URL <https://arxiv.org/abs/2407.07895>. 19

Li, N., Shih, K. J., and Plummer, B. A. Enhancing virtual try-on with synthetic pairs and error-aware noise scheduling, 2025. URL <https://arxiv.org/abs/2501.04666>. 3

Li, P., Xu, Y., Wei, Y., and Yang, Y. Self-correction for human parsing, 2019. URL <https://arxiv.org/abs/1910.09777>. 14, 23

Liang, J., Zeng, H., Cui, M., Xie, X., and Zhang, L. Ppr10k: A large-scale portrait photo retouching dataset with human-region mask and group-level consistency, 2021. URL <https://arxiv.org/abs/2105.09180>. 7, 21, 26

Liu, Z., Luo, P., Qiu, S., Wang, X., and Tang, X. Deepfashion: Powering robust clothes recognition and retrieval with rich annotations. In *2016 IEEE Conference on Computer Vision and Pattern Recognition (CVPR)*, pp. 1096–1104, 2016. doi: 10.1109/CVPR.2016.124. 23

Loshchilov, I. and Hutter, F. Decoupled weight decay regularization, 2019. URL <https://arxiv.org/abs/1711.05101>. 14

Mishchenko, K. and Defazio, A. Prodigy: An expeditiously adaptive parameter-free learner, 2024. URL <https://arxiv.org/abs/2306.06101>. 16

Morelli, D., Fincato, M., Cornia, M., Landi, F., Cesari, F., and Cucchiara, R. Dress code: High-resolution multi-category virtual try-on, 2022. URL <https://arxiv.org/abs/2204.08532>. 7, 8, 14, 16, 25, 29

Morelli, D., Baldrati, A., Cartella, G., Cornia, M., Bertini, M., and Cucchiara, R. Ladi-vton: Latent diffusion textual-inversion enhanced virtual try-on, 2023. URL <https://arxiv.org/abs/2305.13501>. 3

Nam, J., Kim, H., Lee, D., Jin, S., Kim, S., and Chang, S. Dreammatcher: Appearance matching self-attention for semantically-consistent text-to-image personalization. In *Proceedings of the IEEE/CVF Conference on Computer Vision and Pattern Recognition*, pp. 8100–8110, 2024a. 3, 5, 17

Nam, J., Lee, G., Kim, S., Kim, H., Cho, H., Kim, S., and Kim, S. Diffusion model for dense matching, 2024b. URL <https://arxiv.org/abs/2305.19094>. 3, 5

Nam, J., Son, S., Chung, D., Kim, J., Jin, S., Hur, J., and Kim, S. Emergent temporal correspondences from video diffusion transformers. *arXiv preprint arXiv:2506.17220*, 2025a. 3, 5

Nam, J., Son, S., Xu, Z., Shi, J., Liu, D., Liu, F., Kim, S., and Zhou, Y. Visual persona: Foundation model for full-body human customization. In *Proceedings of the Computer Vision and Pattern Recognition Conference*, pp. 18630–18641, 2025b. 2

OpenAI and et al., J. A. Gpt-4 technical report, 2024. URL <https://arxiv.org/abs/2303.08774>. 20

Peebles, W. and Xie, S. Scalable diffusion models with transformers, 2023. URL <https://arxiv.org/abs/2212.09748>. 2, 3

Rombach, R., Blattmann, A., Lorenz, D., Esser, P., and Ommer, B. High-resolution image synthesis with latent diffusion models, 2022. URL <https://arxiv.org/abs/2112.10752>. 3

Shin, C., Choi, J., Kim, H., and Yoon, S. Large-scale text-to-image model with inpainting is a zero-shot subject-driven image generator, 2025. URL <https://arxiv.org/abs/2411.15466>. 4

Siméoni, O., Vo, H. V., Seitzer, M., Baldassarre, F., Oquab, M., Jose, C., Khalidov, V., Szafraniec, M., Yi, S., Ramamonjisoa, M., Massa, F., Haziza, D., Wehrstedt, L., Wang, J., Darzet, T., Moutakanni, T., Sentana, L., Roberts, C., Vedaldi, A., Tolan, J., Brandt, J., Couprie, C., Mairal, J., Jégou, H., Labatut, P., and Bojanowski, P. Dinov3, 2025. URL <https://arxiv.org/abs/2508.10104>. 2, 3, 5, 6, 14, 17

Soloveitchik, M., Diskin, T., Morin, E., and Wiesel, A. Conditional frechet inception distance, 2022. URL <https://arxiv.org/abs/2103.11521>. 19

Su, J., Lu, Y., Pan, S., Murtadha, A., Wen, B., and Liu, Y. Roformer: Enhanced transformer with rotary position embedding, 2023. URL <https://arxiv.org/abs/2104.09864>. 3, 4

Tan, Z., Liu, S., Yang, X., Xue, Q., and Wang, X. Ominicontrol: Minimal and universal control for diffusion transformer, 2025a. URL <https://arxiv.org/abs/2411.15098>. 2, 4

Tan, Z., Xue, Q., Yang, X., Liu, S., and Wang, X. Ominicontrol2: Efficient conditioning for diffusion transformers, 2025b. URL <https://arxiv.org/abs/2503.08280>. 16

Tang, L., Jia, M., Wang, Q., Phoo, C. P., and Hariharan, B. Emergent correspondence from image diffusion, 2023. URL <https://arxiv.org/abs/2306.03881>. 3

Truong, P., Danelljan, M., Yu, F., and Gool, L. V. Warp consistency for unsupervised learning of dense correspondences, 2021. URL <https://arxiv.org/abs/2104.03308>. 3

Tumanyan, N., Geyer, M., Bagon, S., and Dekel, T. Plug-and-play diffusion features for text-driven image-to-image translation, 2022. URL <https://arxiv.org/abs/2211.12572>. 3

Wan, S., Li, Y., Chen, J., Pan, Y., Yao, T., Cao, Y., and Mei, T. Improving virtual try-on with garment-focused diffusion models, 2024. URL <https://arxiv.org/abs/2409.08258>. 3

Wan, S., Chen, J., Pan, Y., Yao, T., and Mei, T. Incorporating visual correspondence into diffusion model for virtual try-on, 2025. URL <https://arxiv.org/abs/2505.16977>. 3

Wang, C., Chen, T., Chen, Z., Huang, Z., Jiang, T., Wang, Q., and Shan, H. Flldm-vton: Faithful latent diffusion model for virtual try-on, 2024. URL <https://arxiv.org/abs/2404.14162>. 3

Xiao, Z., Zhou, Y., Yang, S., and Pan, X. Video diffusion models are training-free motion interpreter and controller, 2024. URL <https://arxiv.org/abs/2405.14864>. 3

Xiaobin, H., Yujie, L., Donghao, L., Xu, P., Jiangning, Z., Junwei, Z., Chengjie, W., and Yanwei, F. Vtbench: Comprehensive benchmark suite towards real-world virtual try-on models, 2025. URL <https://arxiv.org/abs/2505.19571>. 7

Xie, Z., Huang, Z., Dong, X., Zhao, F., Dong, H., Zhang, X., Zhu, F., and Liang, X. Gp-vton: Towards general purpose virtual try-on via collaborative local-flow global-parsing learning, 2023. URL <https://arxiv.org/abs/2303.13756>. 2, 3, 7

Xu, Y., Gu, T., Chen, W., and Chen, C. Ootdiffusion: Outfitting fusion based latent diffusion for controllable virtual try-on, 2024. URL <https://arxiv.org/abs/2403.01779>. 2, 3, 7, 20

Yang, X., Ding, C., Hong, Z., Huang, J., Tao, J., and Xu, X. Texture-preserving diffusion models for high-fidelity virtual try-on, 2024. URL <https://arxiv.org/abs/2404.01089>. 2

Yu, S., Kwak, S., Jang, H., Jeong, J., Huang, J., Shin, J., and Xie, S. Representation alignment for generation: Training diffusion transformers is easier than you think, 2025. URL <https://arxiv.org/abs/2410.06940>. 3, 5, 17

Zhang, R., Isola, P., Efros, A. A., Shechtman, E., and Wang, O. The unreasonable effectiveness of deep features as a perceptual metric, 2018. URL <https://arxiv.org/abs/1801.03924>. 6, 7, 19

Zhang, X., Liao, J., Zhang, S., Meng, F., Wan, X., Yan, J., and Cheng, Y. Videorepa: Learning physics for video generation through relational alignment with foundation models, 2025. URL <https://arxiv.org/abs/2505.23656>. 17

Zhou, Z., Liu, S., Han, X., Liu, H., Ng, K. W., Xie, T., Cong, Y., Li, H., Xu, M., Pérez-Rúa, J.-M., Patel, A., Xiang, T., Shi, M., and He, S. Learning flow fields in attention for controllable person image generation, 2024. URL <https://arxiv.org/abs/2412.08486>. 2, 3

Appendix

This supplementary material provides generalization to additional DiT-based baselines, experimental results, and further applications of our proposed method, CORAL.

- Sec. A presents implementation details of our whole experiments.
- Sec. B provides details on the datasets used in our experiment and the preprocessing pipeline.
- Sec. C extends our analysis and application to additional DiT variants, highlighting the applicability of our CORAL loss.
- Sec. D analyzes computational complexity.
- Sec. E validates our design choice by exploring alternative alignment methods.
- Sec. F describes details of our novel VLM-based evaluation protocol.
- Sec. G reports details and results of human evaluation studies.
- Sec. H presents results on the person-to-person setting to further demonstrate our performance.
- Sec. I presents an additional application of CORAL to person-to-person garment transfer.
- Sec. J provides additional qualitative results.
- Sec. K discusses the limitations of our work and future directions.

A. Implementation Details

A.1. Training Setup

We initialize our model from FLUX.1-Fill-dev and finetune the attention layers. We train with the AdamW (Loshchilov & Hutter, 2019) optimizer using a learning rate of 2×10^{-5} and a batch size of 16 for a total of 8.4k steps on 8 NVIDIA B200 GPUs. We train and report results at a resolution of 1024×768 . For training with $\mathcal{L}_{\text{CORAL}}$, same learning rate and batch size are used, with loss weights $\lambda_{\text{corr}} = 0.01$ and $\lambda_{\text{ent}} = 0.1$. We compute $\mathcal{L}_{\text{CORAL}}$ over all layers throughout training and average it across layers, excluding locations filtered out by the cycle-consistency constraint from the loss computation.

B. Training Dataset

B.1. Dataset Overview

VITON-HD (Choi et al., 2021) comprises 11,647 training images and 2,032 test images and focuses on upper-body garments captured in a studio setting. DressCode (Morelli et al., 2022) consists of 48,392 training set and 5,400 test set, covering 13,563 upper, 7,151 lower and 27,678 dresses. The person images are generally full-body centered, with face region excluded. In both datasets, garment product images are typically captured on plain, white backgrounds and presented as flat product shots. Overall, person images in both benchmarks are captured under controlled backgrounds and lighting, and most samples present static, frontal poses with limited viewpoint variation.

B.2. Dataset Preprocessing

We follow prior works (Chong et al., 2025; Huang et al., 2024) for input prompts, using a fixed input prompt for VITON-HD and adding the garment category for DressCode. For VITON-HD, we use both the masks from benchmarks and ones preprocessed by prior work (Choi et al., 2024) in a 1:1 ratio. For DressCode, we adopt masks preprocessed by prior work (Choi et al., 2024), and at each training step we apply a random directional dilation with a radius uniformly sampled from 1 to 20 pixels to augment the masks. Input masks can cover cloth-agnostic regions such as hair or bags, which makes it difficult to preserve their appearance from the input under occlusions. While one could refine the masks to exclude such regions, this comes with practical risks: if the masks become too tight, they can reveal the originally worn garment, while accurately segmenting fine structures such as hair across diverse poses and viewpoints is often costly and error-prone. Instead, we extract these regions using human-parser (Li et al., 2019) or SAM3 (Carion et al., 2025), and provide them as additional guidance by stitching them into the DensePose (Güler et al., 2018) condition. We construct pseudo ground-truth correspondences using DINOv3-B (Siméoni et al., 2025) and set the cycle-consistency threshold γ as 3.

C. CORAL on Other Baselines

CORAL is designed to be model-agnostic and can be plugged in any DiT architecture that exposes a person \rightarrow attention map for supervision. To demonstrate this, we extend our application to additional DiT baseline.

C.1. Baselines with Different Pose Injection Strategies

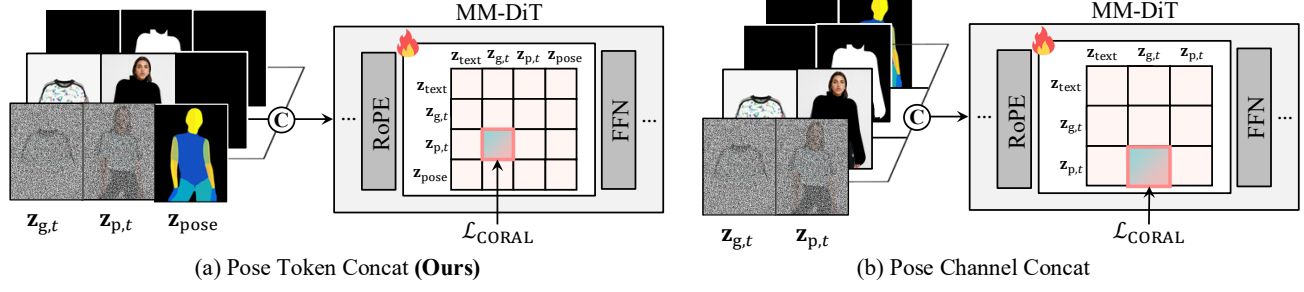


Figure C.1. Architecture Comparison.

Pose Token Concat. To leverage the DiT’s token-based processing over the full sequence, we consider a baseline that injects pose as additional tokens. As shown in Fig. C.1 (a), we concatenate the pose condition z_{pose} along the token dimension. This preserves positional structure in the token space and provides explicit pose correspondences to the model. Our main experiments use this **Pose Token Concat.** baseline. For more details, see Sec. 4.2 of the main paper and Sec. A of Appendix.

Pose Channel Concat. As illustrated in Fig. C.1 (b), we additionally design a baseline that injects the pose condition z_{pose} along the channel dimension rather than the token dimension. Specifically, we first form a pose diptych $z_{\text{pose-diptych}}$ by placing z_{pose} next to a zero-padded panel to match the diptych layout. We then concatenate z_t , z_{diptych} , m_{diptych} , and the $z_{\text{pose-diptych}}$ channel-wise, and feed the resulting tokens to the input projection layer within FLUX.1-Fill-dev. This increases the projection input dimension from 384 to 448, so we expand the projection layer and zero-initialize the newly added weights. Copying the original projection weights into the expanded channels led to degraded performance and unstable convergence.

Table C.1. Effect of $\mathcal{L}_{\text{CORAL}}$ across Baselines with Different Pose Injection Strategies for VITON-HD (Choi et al., 2021).

Methods	$\mathcal{L}_{\text{CORAL}}$	Paired				Unpaired	
		SSIM \uparrow	LPIPS \downarrow	FID \downarrow	KID \downarrow	FID \downarrow	KID \downarrow
Pose Token Concat	\times	0.889	0.055	5.543	0.870	9.641	1.323
	\checkmark	0.907 (+2.02%)	0.048 (+12.73%)	4.962 (+10.48%)	0.565 (+35.06%)	8.763 (+9.11%)	0.880 (+33.48%)
Pose Channel Concat	\times	0.886	0.060	5.554	0.540	9.841	1.221
	\checkmark	0.888 (+0.23%)	0.059 (+1.67%)	5.372 (+3.28%)	0.744	9.323 (+5.26%)	1.077 (+11.79%)

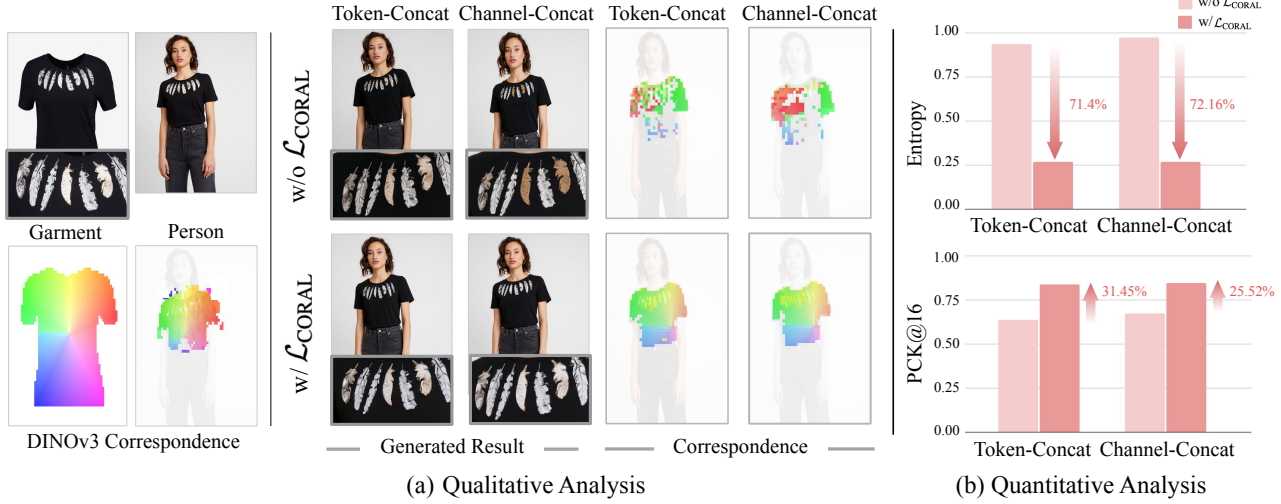


Figure C.2. Effect of $\mathcal{L}_{\text{CORAL}}$ across Baselines with Different Pose Injection Strategies.

Effect of $\mathcal{L}_{\text{CORAL}}$. We evaluate CORAL on two pose-injection baselines, **Pose Token Concat.** and **Pose Channel Concat.**, with and without $\mathcal{L}_{\text{CORAL}}$. As reported in Tab. C.1, adding $\mathcal{L}_{\text{CORAL}}$ consistently improves VTON performance for both baselines, demonstrating that CORAL is model-agnostic across DiT variants that expose a person→garment attention. Between the two baselines, Pose Token Concat performs notably better than Pose Channel Concat. This is expected because token concatenation preserves spatially aligned pose tokens that the DiT can attend to directly, whereas channel concatenation injects pose more indirectly through the input projection. Fig. C.2 (a) further shows that $\mathcal{L}_{\text{CORAL}}$ refines person→garment mismatches in attention, leading to more accurate garment transfer: for instance, the fourth and fifth feather patterns no longer bleed into nearby brown tones and remain clean white as in the garment reference. Fig. C.2 (b) quantitatively supports that across both baselines, $\mathcal{L}_{\text{CORAL}}$ reduces attention entropy and increases PCK, indicating sharper and more correct correspondences.

C.2. An Additional Efficient Baseline

We introduce an additional efficient baseline trained under a different setup to test whether CORAL’s improvements remain consistent beyond the settings in Sec. C.1 .

Architectural Details. Additional baseline is designed to be computationally efficient. Following the compact token integration method in prior work (Tan et al., 2025b), we first restrict denoising processes to the garment region in \mathbf{z}_p using downsampled mask \mathbf{m}_e , since denoising the full person latent adds unnecessary computation and can also perturb garment-unrelated areas. At diffusion timestep t , the noisy person latent is defined as:

$$\mathbf{z}_{p,t} = \left((1-t)\mathbf{z}_p + t\epsilon \right) \odot \mathbf{m}_p + \mathbf{z}_p \odot (1 - \mathbf{m}_p). \quad (21)$$

We also keep the garment latent clean to avoid unnecessary denoising process on the garment input. For pose conditioning, we concatenate the pose condition \mathbf{z}_{pose} along the token dimension, as discussed in Sec. 4.2.

Implementation Details. We initialize our model from `FLUX.1-dev` and finetune with LoRA (Hu et al., 2021) with rank 128. We train with Prodigy (Mishchenko & Defazio, 2024) optimizer using a learning rate of 1.0 and batch size of 1 on 2 NVIDIA A100 GPUs. We train and report results at a resolution of 1024 x 1024. For training with $\mathcal{L}_{\text{CORAL}}$, same learning rate and batch size are used, with loss weights $\lambda_{\text{corr}} = 0.01$ and $\lambda_{\text{ent}} = 0.1$. All other implementation details follow Sec. A of Appendix.

Table C.2. Effect of $\mathcal{L}_{\text{CORAL}}$ on Additional Efficient Baseline for VITON-HD (Choi et al., 2021) and DressCode (Morelli et al., 2022).

$\mathcal{L}_{\text{CORAL}}$	VITON-HD						DressCode					
	Paired			Unpaired			Paired			Unpaired		
	SSIM \uparrow	LPIPS \downarrow	FID \downarrow	KID \downarrow	FID \downarrow	KID \downarrow	SSIM \uparrow	LPIPS \downarrow	FID \downarrow	KID \downarrow	FID \downarrow	KID \downarrow
✗	0.864	0.084	9.521	1.353	11.251	0.456	0.905	0.065	5.752	0.473	8.723	0.736
✓	0.871 (+0.81%)	0.084	6.271 (+34.1%)	0.563 (+58.5%)	10.285 (+8.62%)	0.315 (+30.9%)	0.905	0.061 (+6.15%)	5.221 (+9.22%)	0.581	8.70 (+0.23%)	0.193 (+73.78%)

Effect of $\mathcal{L}_{\text{CORAL}}$. Applying CORAL improves the efficient baseline across overall metrics, with particularly large improvements compared to our main baseline. In this efficient training setup with LoRA finetuning, the baseline performance is relatively weaker, yet CORAL still yields substantial gains. The largest improvements appear in distribution-based metrics, which indicates that CORAL also enhances overall realism of generated outputs, not only the perceptual fidelity. Overall, the improvements across baselines confirm the effectiveness of $\mathcal{L}_{\text{CORAL}}$ and highlight its suitability for DiTs, where attention provides an explicit controllable correspondence mechanism.

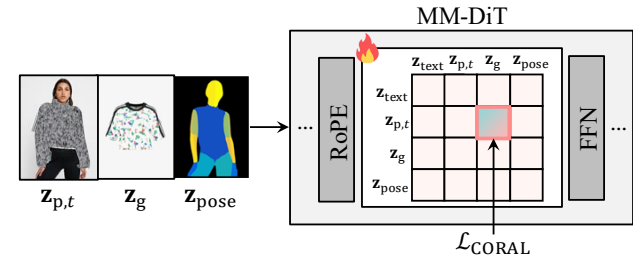


Figure C.3. Efficient Baseline Architecture.

D. Runtime and Memory

In Table C.3, we report the hardware setup, throughput, and peak GPU memory for each baseline setting.

Table C.3. Speed and memory. T denotes training and I denotes inference. Speed is in img/sec and VRAM is in GB.

Setting	$\mathcal{L}_{\text{CORAL}}$	GPU	GPU# (T/I)	Batch (T/I)	Speed (T/I)	VRAM (T/I)
Token-concat	✓	B200	8 / 1	16 / 1	2.61 / 0.091	148 / 40
Token-concat	✗	B200	8 / 1	16 / 1	3.01 / 0.105	148 / 40
Channel-concat	✓	B200	8 / 1	16 / 1	3.41 / 0.119	148 / 40
Channel-concat	✗	B200	8 / 1	16 / 1	3.92 / 0.137	148 / 40
Efficient	✓	A100	1 / 1	1 / 1	0.16 / 0.025	48 / 33
Efficient	✗	A100	1 / 1	1 / 1	0.18 / 0.025	48 / 33

E. Additional Analysis

E.1. Alignment Target

Table E.4. Alignment Target Ablation on VITON-HD (Choi et al., 2021).

Methods	Paired				Unpaired	
	SSIM \uparrow	LPIPS \downarrow	FID \downarrow	KID \downarrow	FID \downarrow	KID \downarrow
(I) Baseline	0.889	0.055	5.543	0.870	9.641	1.323
(II) (I) + Feature Alignment (REPA) (Yu et al., 2025)	0.885 (-0.45%)	0.087 (-58.18%)	13.718 (-147.48%)	2.103 (-141.72%)	15.621 (-62.03%)	3.684 (-178.46%)
(III) (I) + Query-Key Correspondence Alignment (Ours)	0.907 (+2.02%)	0.048 (+12.73%)	4.962 (+10.48%)	0.565 (+35.06%)	8.763 (+9.11%)	0.880 (+33.48%)

We compare two alignment methods for improving person-garment correspondence during training. The first aligns intermediate DiT features to the feature descriptors $\phi(\cdot)$ from DINOv3, using cosine similarity loss, following prior work (Yu et al., 2025). The second is our method, CORAL, which aligns attention-derived correspondences by supervising query-key matches. Motivated by prior analyses that query-key similarities largely determine the spatial arrangement of generated image elements while value features mainly carry appearance details (Nam et al., 2024a), we align query-key correspondences to correct spatial matching, without altering the model’s learned appearance representation. Prior work (Zhang et al., 2025) emphasizes that direct feature alignment method (Yu et al., 2025) is designed to accelerate training from scratch, rather than to transfer a pretrained model through fine-tuning. Such hard alignment pulls intermediate DiT features toward DINOv3 features, which can disrupt inherent generative representation learned during pretraining and lead to slower convergence. We evaluate this direct feature alignment baseline in our setting and report the results.



Figure E.4. Intermediate Feature Alignment vs. Ours.

Implementation Details on Feature Alignment. We build the intermediate feature alignment baseline upon the same architectural modifications adopted in our main baseline described in Section 4.2. To align intermediate representations within DiTs with external semantic features, we follow the prior work (Yu et al., 2025), which aligns transformer features with representations extracted from a pretrained vision encoder. We use DINOv3-B (Siméoni et al., 2025) as the external encoder, consistent with our main baseline.

We attach a lightweight projection head to the output of each transformer block. Each head is a three-layer MLP with SiLU activations that maps DiT hidden states into the DINOv3 embedding space.

Given a garment image I_g and a person image I_p , we concatenate them horizontally to form $\hat{I} \in \mathbb{R}^{H \times 2W \times 3}$, and extract

DINOv3 features $\phi_g, \phi_p \in \mathbb{R}^{hw \times 768}$ from the frozen encoder. We concatenate them as:

$$\hat{\phi} = [\phi_g \parallel \phi_p] \in \mathbb{R}^{2hw \times 768}. \quad (22)$$

Let \mathbf{h} be an intermediate hidden representation from the diffusion transformer \mathbf{v}_θ , and let $f_\omega(\cdot)$ be a trainable projection head. We define a patch-wise alignment loss:

$$\mathcal{L}_{\text{REPA}}(\theta, \omega) := -\mathbb{E}_{\hat{I}, \epsilon, t} \left[\frac{1}{K} \sum_{k=1}^K \text{sim}(\hat{\phi}_k, f_\omega(\mathbf{h}_k)) \right], \quad (23)$$

where k indexes patches and K is the number of patches. We compute this loss at the output of each transformer block using its corresponding projection head, and average it across layers.

The final objective adds the projection loss to the standard flow-matching loss:

$$\mathcal{L}_{\text{total}} = \mathcal{L}_{\text{velocity}} + \lambda_{\text{REPA}} \mathcal{L}_{\text{REPA}}, \quad (24)$$

where we set $\lambda_{\text{REPA}} = 0.1$ in all experiments.

Comparison & Analysis. Table E.4 compares the two alignment methods, showing that CORAL achieves better try-on quality with higher SSIM and lower LPIPS. Correspondence-based VTON methods leverage feature-level alignment or feature-based matching to transfer garments (Chen et al., 2024; Huang et al., 2022). Prior analyses suggest that query–key similarity is closely tied to spatial correspondence, while value pathways are more related to appearance. Since intermediate features jointly encode both information, directly aligning them can also affect the inherent representations learned during pretraining. By supervising query key matches, CORAL strengthens person garment alignment while largely preserving the model’s learned appearance representation. In contrast, feature-level alignment shows a larger change in intermediate features, followed by a substantial performance drop across all metrics in Tab. E.4 and misaligned texture in Fig. E.4.

F. VLM-based Evaluation

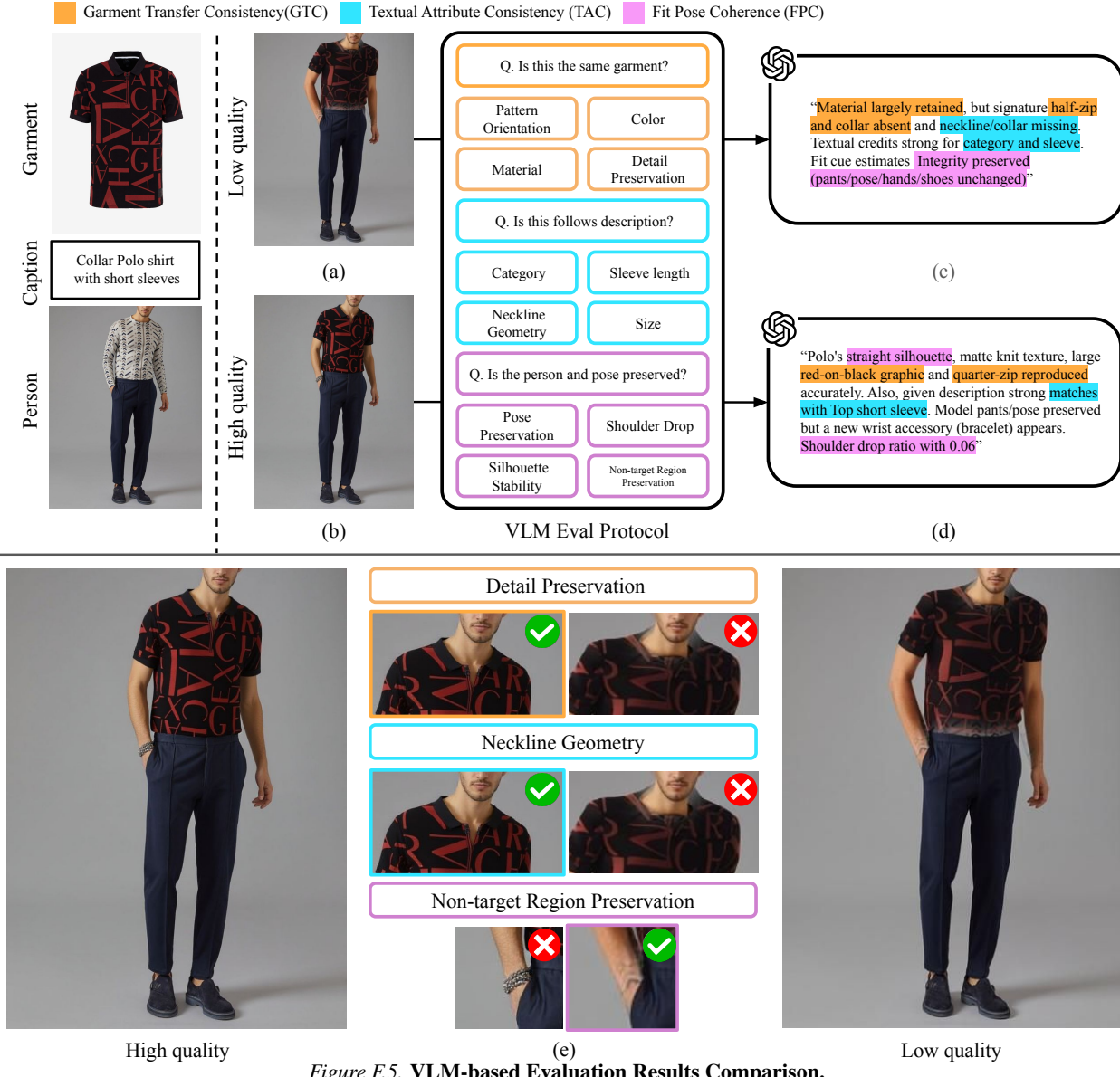


Figure F.5. VLM-based Evaluation Results Comparison.

Why VLM-based Evaluation is Needed? As discussed in Sec. 5.1, standard metrics such as FID (Soloveitchik et al., 2022), KID (Bińkowski et al., 2021), SSIM (Cong et al., 2022) and LPIPS (Zhang et al., 2018) are insufficient for evaluating VTON, as they mainly reflect overall realism or low-level similarity and do not assess whether the specific reference garment is faithfully transferred and plausibly worn. Following Sec. 5.1 of the main paper, we therefore propose a VLM-based evaluation protocol with three criteria, including Garment Transfer Consistency (GTC), Textual Attribute Consistency (TAC), and Fit Pose Coherence (FPC). For all VLM-based evaluations, we use GPT-5 mini as our evaluator. The full input prompt used for VLM evaluation is provided in the Fig. K.18.

Fig. F.5 motivates the need for this protocol. Although the two outputs in Fig. F.5 (a) and (b) are generated from the same input garment and person, they differ in whether garment details, attributes and fit-pose are preserved. Our evaluator produces GTC, TAC, and FPC scores together with natural language justifications that explain which visual evidence supports each score, as shown in Fig. F.5 (c) and (d). (e) provides the detailed view of the generated images aligned with each criterion. This design is motivated by recent findings (Cheng et al., 2025; Jia et al., 2025; Chen et al., 2025) that VLMs (Dai et al., 2023; Li et al., 2024) excel at image and multi-image reasoning, making them well suited to judge garment-specific fidelity beyond distribution-level similarity.

G. Human Evaluation

Human Evaluation Details. We conducted a user study to measure virtual try-on quality under human perception and to validate that our VLM-based evaluation reflects human preference. Participants rated each generated result on the same three criteria used in Sec. 5.1, including Garment Transfer Consistency (GTC), Textual Attribute Consistency (TAC), and Fit-Pose Coherence (FPC), using a 5-point scale (from 1 to 5) for each criterion. Fig. K.17 presents example questions from the user study.

To make the criteria concrete and reduce ambiguity, we provided references for each question. For GTC, we showed the input garment image so participants could directly compare whether shape, patterns, and logos were preserved. For TAC, we provided a short textual description of the garment attributes, automatically extracted from the reference garment using a pretrained vision-language model (OpenAI & et al., 2024). For FPC, we showed the input person image so participants could judge whether the garment is worn naturally and follows the target pose and body geometry without altering non-target regions.

A total of 54 participants answers 45 questions. For a fair comparison, we sampled outputs from a large pool sharing the same input person image and garment image across 5 comparison models, including OOTDiffusion (Xu et al., 2024), IDM-VTON (Choi et al., 2024), CatVTON (Chong et al., 2025), Any2AnyTryOn (Guo et al., 2025) and CORAL (Ours) to ensure intra-rater reliability.

Human Evaluation Results. Fig. G.6 shows the results, demonstrating that our model outperforms others across all criteria.

Correlation with VLM-Evaluation. We find that our VLM-based scores align well with the user study outcomes, indicating that the proposed VLM evaluation reflects human preference more faithfully than standard metrics. In both Tab. 4, methods that receive higher GTC/TAC/FPC scores also tend to be preferred by human participants, and CORAL performs strongly in both evaluations. This agreement suggests that GTC, TAC, and FPC capture perceptually important failure cases in try-on quality.

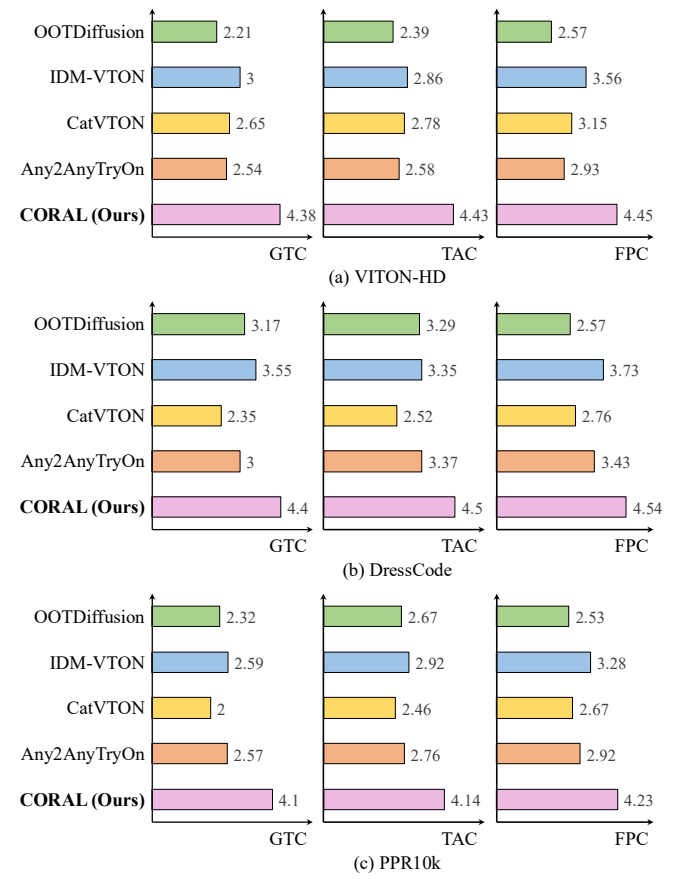


Figure G.6. User Study Results.

H. Evaluation on Additional Datasets

H.1. Motivation

We evaluate whether the correspondences learned by CORAL generalize beyond standard VTON benchmarks and still leads to high-quality try-on results under input conditions that are less curated than the benchmark setting. For the person input, we consider photos with broader variation in poses, viewpoints, backgrounds, framing, and occlusions than typical benchmarks. For the garment input, we consider reference images that are not limited to clean product images.

Most existing VTON benchmarks follow the in-shop garment transfer setting, where the reference garment is a flat product image and the target person is photographed in a controlled studio environment. However, this setting does not fully reflect real-world inputs. User-provided person photos are often taken in everyday environments with diverse framing, non-frontal viewpoints, more dynamic poses, and frequent occlusions by accessories or surrounding objects. Garment reference images can also differ substantially in practice. It is often inconvenient for users to search for and provide a clean product photo for every garment. Instead, they typically rely on readily available photos, such as a casually taken garment photo with cluttered backgrounds or a worn-garment image from another person, which introduces additional noises compared to product images.

For this reason, we additionally build paired and unpaired test sets to evaluate CORAL under more challenging conditions while keeping the evaluation reliable. We evaluate with worn-garment references, where the reference garment is worn by another person, which is typically more challenging than a clean product image but still provides sufficient garment cues for try-on.

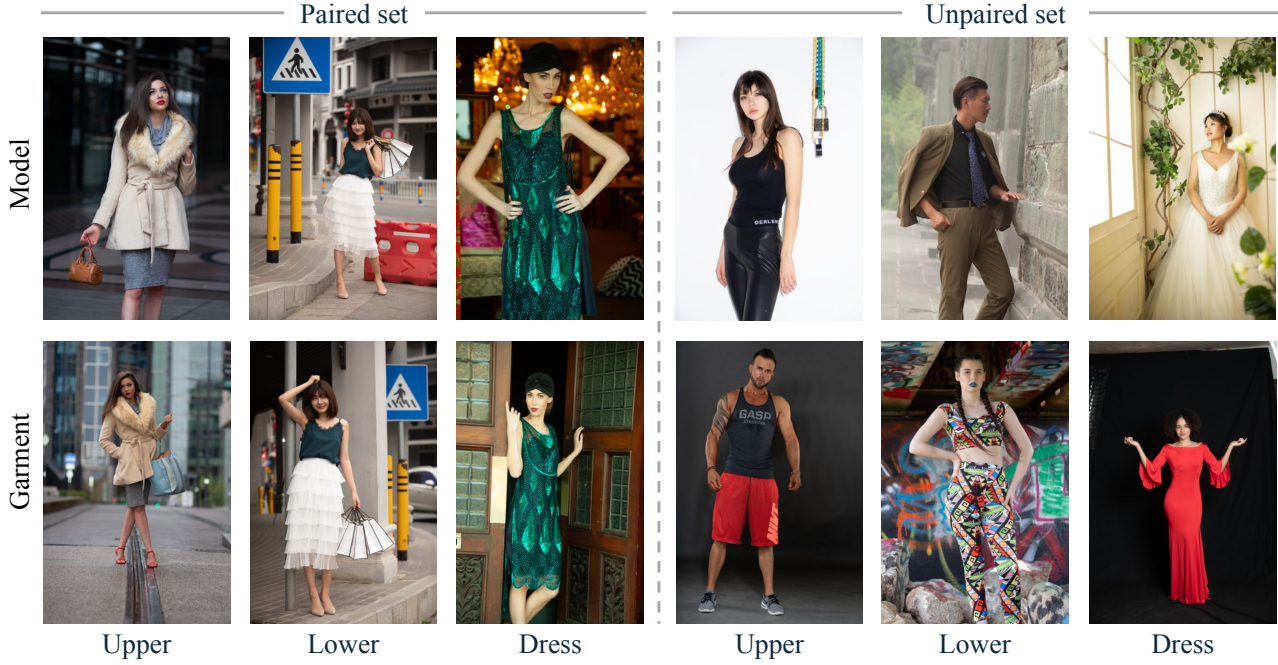


Figure H.7. Additional Evaluation Dataset Samples.

H.2. Evaluation Dataset Details

We additionally build paired and unpaired evaluation sets using PPR10K (Liang et al., 2021), since it offers high-resolution full-body portraits captured under diverse real-world conditions and provides grouped images of the same subject, which enables stable paired evaluation with consistent garment identity.

Dataset Overview. PPR10K is a large scale, high quality portrait photo retouching dataset designed to cover diverse real world conditions. It contains 11,161 high resolution raw portrait photos organized into 1,681 groups, where each group includes 3 to 18 photos of the same subject captured in the same scene within a short time span. The dataset was curated to cover diverse shooting purposes such as weddings, graduations, and advertisements. It also includes diverse subjects (e.g., children and people from diverse regions), varied indoor and outdoor backgrounds, and a wide range of lighting conditions

from day to night and across seasons. The portraits cover diverse framing from face-centric to full-body shots, and include various viewpoints excluding fully back-facing.

Dataset Preprocessing. We first filter person images to keep upper-body to full-body shots. We remove face-centric crops by extracting 2D keypoints with OpenPose (Cao et al., 2021) and retaining images where the body is visible at least down to the knees. We further heuristically filter samples by viewpoints using IUV maps extracted from DensePose (Güler et al., 2018) to exclude fully back and side views. For the reference garment setting, we exclude images where the garment region is too small to provide meaningful detail, as well as extreme cases such as overly dark or overexposed images and heavy occlusions. We use the same preprocessing pipeline as in the standard VTON benchmarks for extracting DensePose conditions. We obtain input masks following prior work (Choi et al., 2024). After preprocessing, the final split contains 358 dresses, 320 upper-body samples, and 195 lower-body samples. In the paired setting there are 309 samples (138 dresses, 86 upper-body, 85 lower-body) and in the unpaired setting there are 564 samples (220 dresses, 234 upper-body, 110 lower-body).

I. Person-To-Person Garment Transfer

Motivation. As mentioned in Sec. H.1, worn-garment transfer is a practically important setting where the garment is observed on another clothed person rather than as a clean product photo. We refer to this setup as *person-to-person* garment transfer. Compared to in-shop product photos, worn-garment references are more common in real world and also show how the garment looks when worn, but it is harder to determine what should be transferred from in-the-wild reference images. A standard in-shop setting often addresses this by estimating a garment mask from the reference image of a clothed person, but this mask can be unreliable under heavy occlusions or complex backgrounds. As illustrated in the first row of Fig. I.8, occlusion by hair can remove garment regions in the mask, and the try-on result can transfer this missing shape, making the garment look cut out in the same area. Garment masks can also remove global shape information such as overall length and silhouette, which is particularly critical for lower-garment transfer. As shown in Fig. I.8, for skirts and dresses, a garment-only reference cropped by a mask can hide where the garment ends on the body, making it difficult to preserve the correct length. For this reason, we train a separate model for *person-to-person* garment transfer using full reference images without estimating garment masks, and apply CORAL to improve person–garment correspondence under these in-the-wild references.

Architectural Details. In the *person-to-person* garment transfer setting, the garment reference image is provided through another clothed person image rather than a clean product image. We therefore denote the target and reference person images as $I_{p_{tgt}}$ and $I_{p_{ref}}$, and encode them with a VAE to obtain the corresponding latents $\mathbf{z}_{p_{tgt}}$ and $\mathbf{z}_{p_{ref}}$. Following the same diptych layout as in Sec. 4.2, at diffusion timestep t , we construct the noisy diptych latent as:

$$\mathbf{z}_t = [\mathbf{z}_{p_{ref},t} \parallel \mathbf{z}_{p_{tgt},t}]. \quad (25)$$

For conditioning worn-garment reference image and the masked person image, we use the clean reference person latent and the masked target person latent as:

$$\mathbf{z}_{\text{diptych}} = [\mathbf{z}_{p_{ref}} \parallel \mathbf{z}_{p_{tgt}} \odot (1 - \mathbf{m}_e)], \quad (26)$$

where \mathbf{m}_e is obtained by downsampling M_e into the latent space. We use the same definition of the binary mask canvas $\mathbf{m}_{\text{diptych}}$ as in Sec. 4.2.

Since DensePose (Güler et al., 2018) can be estimated from both $I_{p_{tgt}}$ and $I_{p_{ref}}$, we extract two pose conditions aligned to the target and reference persons, denoted as $I_{\text{pose}_{tgt}}$ and $I_{\text{pose}_{ref}}$, and then encode them with a VAE to obtain $\mathbf{z}_{\text{pose}_{tgt}}$ and $\mathbf{z}_{\text{pose}_{ref}}$.

Due to additional pose inputs for the reference worn-garment image, pose injection through token concatenation would increase the number of tokens, leading to higher computation and memory cost. We therefore inject the pose condition along the channel dimension instead. As explained in Sec. C.1 of Appendix, we build the diptych layout for pose conditions, $\mathbf{z}_{\text{pose-diptych}} = [\mathbf{z}_{\text{pose}_{\text{ref}}} \parallel \mathbf{z}_{\text{pose}_{\text{tgt}}}]$, and then concatenate \mathbf{z}_t , $\mathbf{z}_{\text{diptych}}$, $\mathbf{m}_{\text{diptych}}$, and the $\mathbf{z}_{\text{pose-diptych}}$ channel-wise before the input projection layer in FLUX.1-Fill-dev.

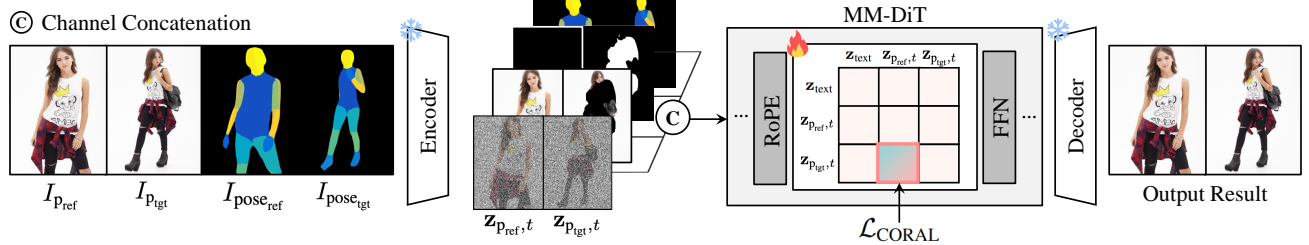


Figure I.9. Person-To-Person Architecture.

Training Dataset. Existing VTON benchmarks are built on curated paired sets where the reference image is a flat in-shop product image, typically centered with a clean background. The worn-garment setting, however, does not come with an established benchmark. Even though some public paired datasets are available where multiple subject images share the same garment identity, some images have incorrect garment identity annotations, and there is no annotation indicating which image in each group should be used as the reference worn-garment image. In the worn-garment setting, many images are in-the-wild with different viewpoints, framing, and occasional occlusions, so some images may include garments that are not visible enough to be used as a reliable reference input.

To build paired data for *person-to-person* garment transfer, we leverage DeepFashion (Liu et al., 2016) and an internal dataset. DeepFashion provides 14,120 pairs for the multi-view try-on task, and each pair typically includes multiple viewpoints across a range of garment categories, with reliable garment identity annotations. We filter out reference images with extreme viewpoints such as strong side or back views using DensePose (Güler et al., 2018) IUV maps, and overly tight crops using human parsing maps (Li et al., 2019). We also leverage an internal dataset covering tops, bottoms, and dresses, where images are paired by garment identity across different subjects, with garment identities annotated by human annotators. For in-the-wild images that are not full body, human parsing or OpenPose (Cao et al., 2021) can fail, so we additionally use SAM3 (Carion et al., 2025) to generate the input masks. In total, our final training set contains 23,678 paired samples.

Quantitative Results. As shown in Tab. I.5, training the model for *person-to-person* garment transfer with worn-garment references achieves better performance than using a model trained with in-shop product photos without retraining. In Tab. I.5, **CORAL-P2P** uses the unmasked reference image at inference time, while the other **CORAL** settings use a garment-only reference extracted with a garment mask. In this more challenging setting, $\mathcal{L}_{\text{CORAL}}$ helps the model focus on the intended garment and avoid transferring details from irrelevant parts of the reference image, which is reflected in the quantitative results of Tab. I.5 across both paired and unpaired settings.

Qualitative Results. We provide qualitative results for the *person-to-person* garment transfer in Fig. I.8 and Fig. I.10. Models trained with in-shop product images often struggle when the garment reference is provided as a clothed person image rather than a clean product photo. As shown in Fig. I.8, the visible garment region in the reference image can be incomplete under occlusion, and the generated try-on result follow the edge of visible part, making the garment look cut off or visually deformed. Training on *person-to-person* pairs helps the model produce a more natural garment shape even under such occlusions, where the shoulder part in shirts is generated seamlessly with **CORAL-P2P**. For lower garments and dresses, garment length is hard to infer from a garment-only reference cropped by a mask, since it removes global information about where the garment ends on the body and its overall silhouette, which can lead to shortened hems or incorrect length, as shown in Fig. I.8. Instead, Fig. I.10 further shows that **CORAL-P2P** preserves overall length and silhouette by conditioning on the full reference person image, keeping the skirt length just above the ankles, as in the reference.

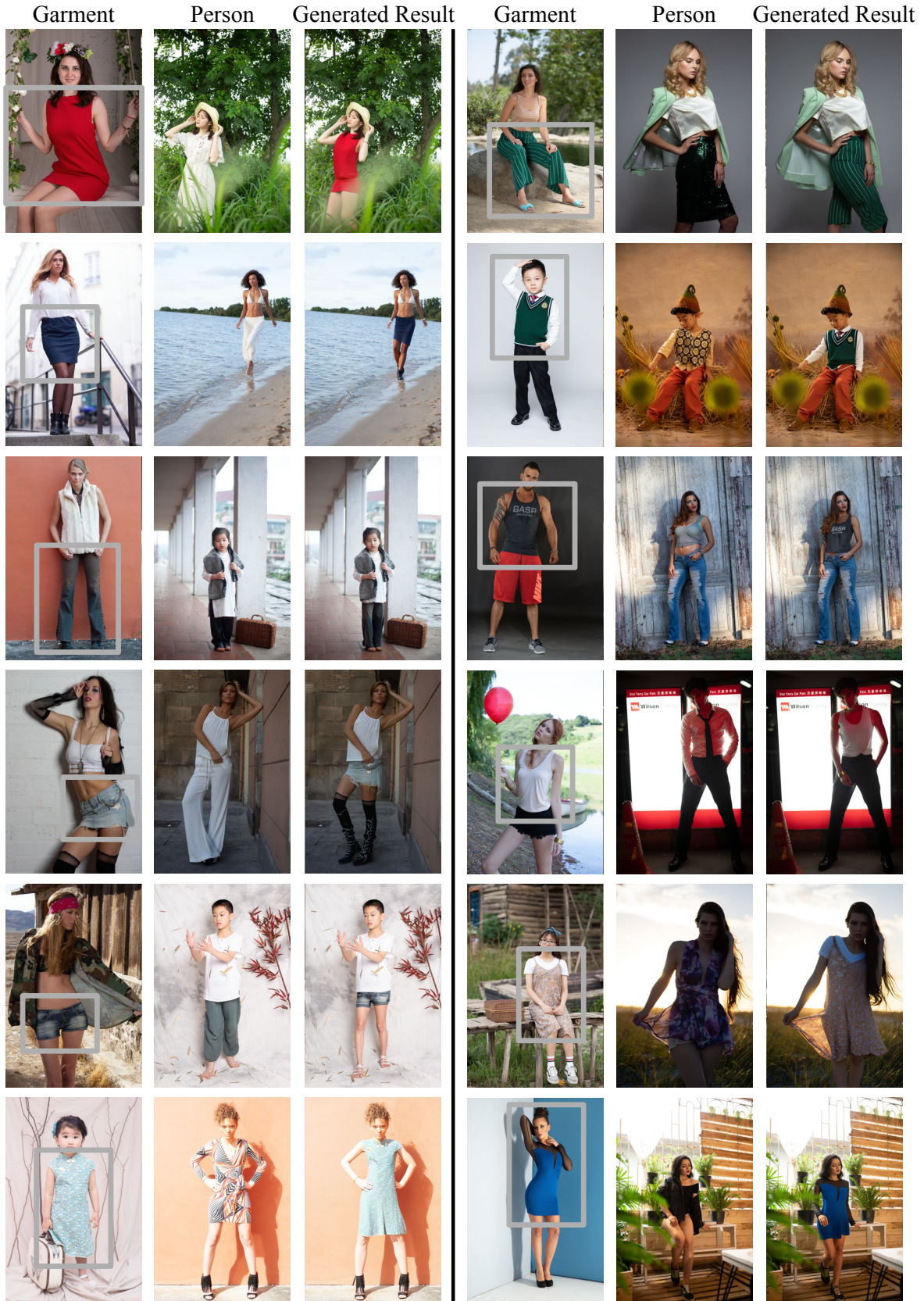


Figure I.10. Qualitative Results of CORAL-P2P on PPR10K.

J. Additional Qualitative Results

We further compare CORAL with recent VTON methods on standard benchmarks and in-the-wild dataset in Fig. J.11, Fig. J.12, and Fig. J.13. We also report results for the baseline model trained without $\mathcal{L}_{\text{CORAL}}$ and with $\mathcal{L}_{\text{CORAL}}$, showing that CORAL consistently improves try-on quality by enhancing person–garment alignment and reducing misplacement artifacts in Fig. J.15 and Fig. J.16. We additionally evaluate CORAL on PPR10K to assess the generalization of our model trained only on standard virtual try on benchmarks in Fig. J.14.

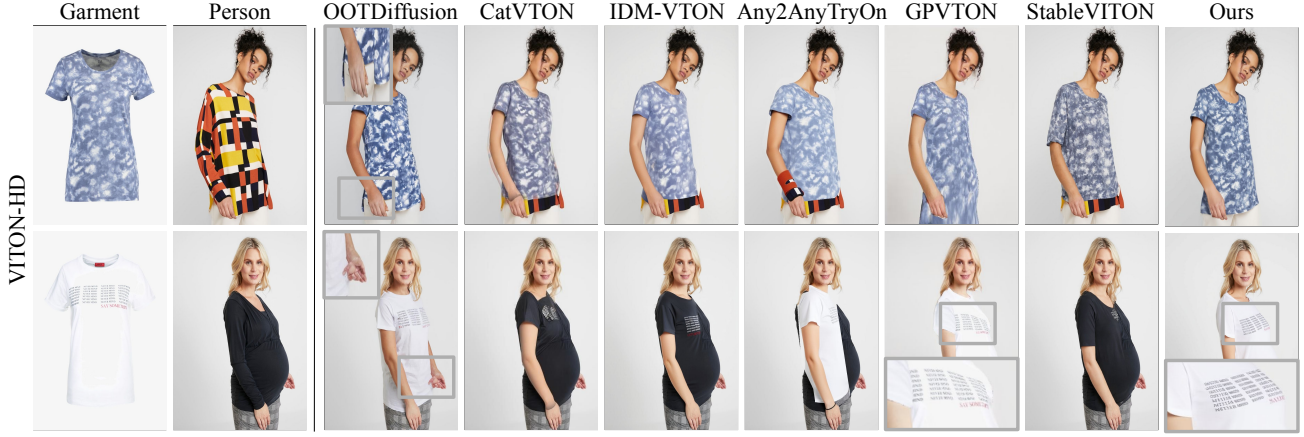


Figure J.11. Additional Qualitative Comparison of CORAL on VITON-HD (Choi et al., 2021).



Figure J.12. Additional Qualitative Comparison of CORAL on DressCode (Morelli et al., 2022).



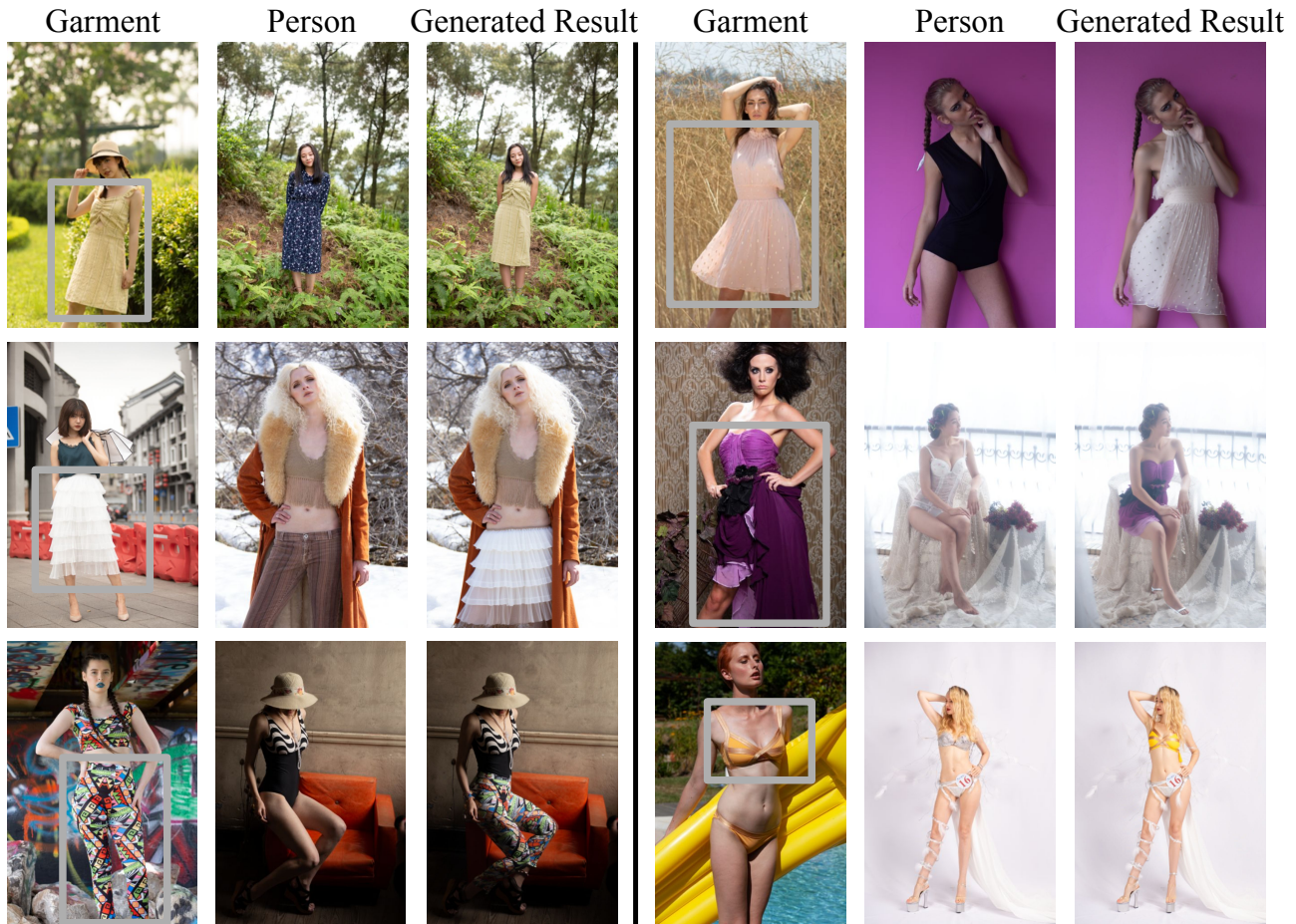


Figure J.14. Additional Qualitative Results of CORAL on PPR10K.

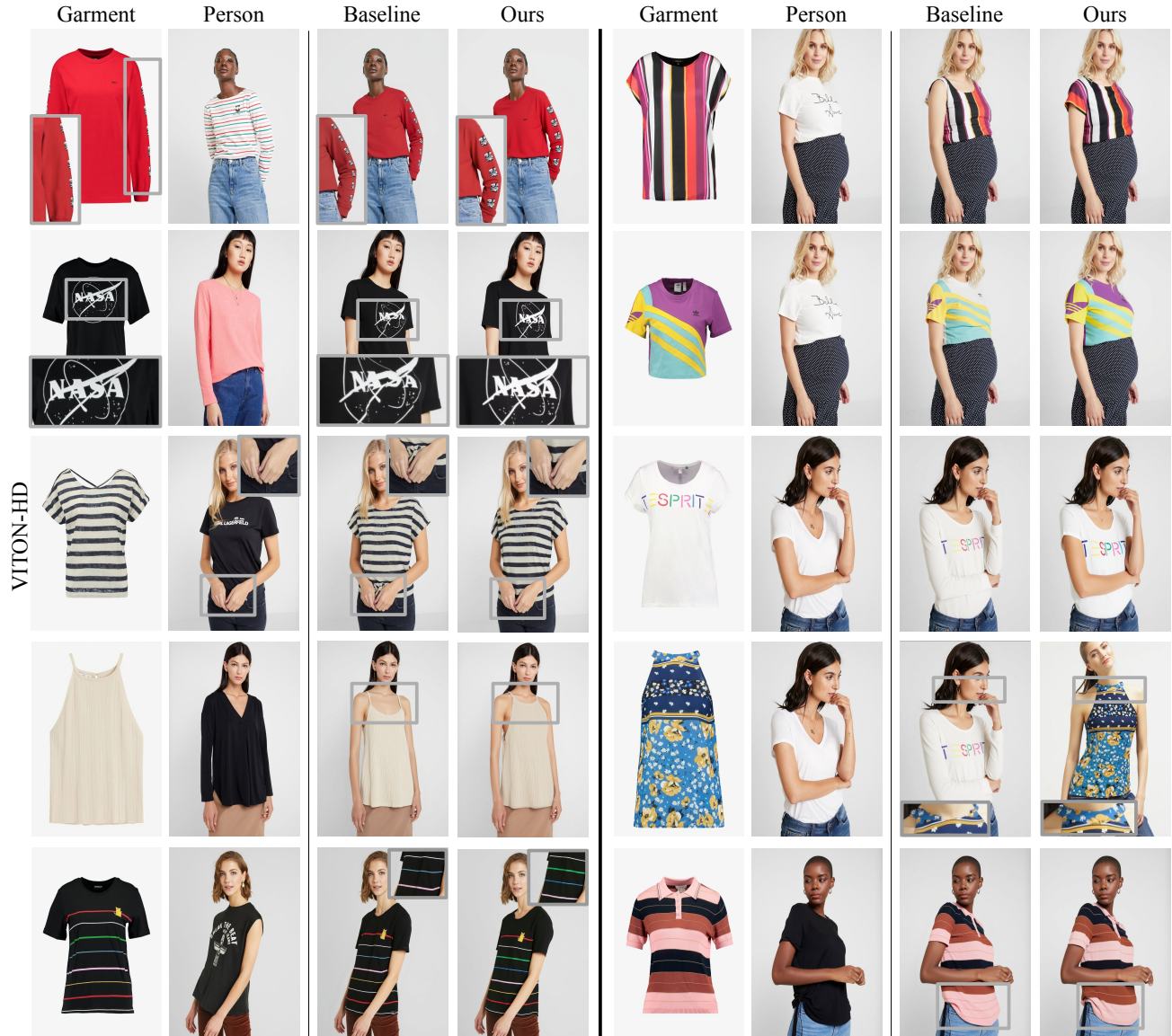


Figure J.15. Qualitative Comparisons on VITON-HD (Choi et al., 2021) Before and After CORAL Loss.

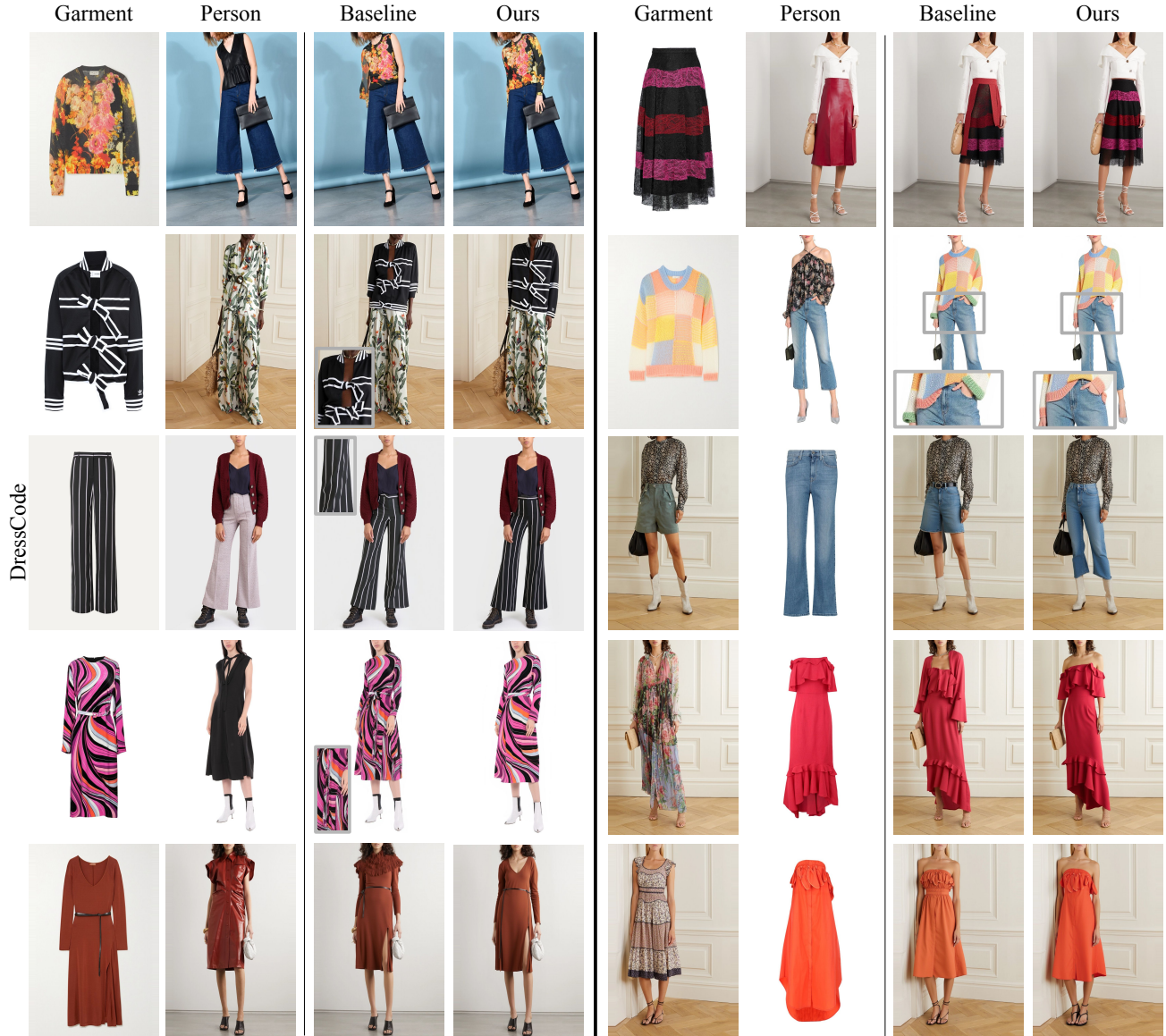


Figure J.16. Qualitative Comparisons on DressCode (Morelli et al., 2022) Before and After CORAL Loss.

K. Limitations and Discussion

Reliance on DINOv3 Pseudo Ground-Truth. CORAL supervises query–key matching using DINOv3-based pseudo ground-truth correspondences, so its correspondence quality can degrade when DINOv3 matching is unreliable, such as under strong appearance changes, heavy occlusions, or extreme viewpoints. While our cycle-consistency based reliability filtering removes many unstable matches, some noisy matches may remain and occasionally lead to incorrect supervision. A promising direction is to incorporate stronger confidence modeling, aggregate pseudo matches from multiple matching models, or introduce self-consistency checks to further reduce the impact of noisy pseudo labels.

Efficiency. Our baseline injects pose by concatenating pose latents along the token dimension, which increases the sequence length and can raise the training cost. In practice, this overhead can be reduced by using a compact pose representation.

Future Directions. Although we focus on VTON, an important future direction is to extend CORAL to broader reference-image-based customization settings, where a reference image specifies the target appearance while preserving the input content and structure. We also expect that leveraging stronger pseudo-correspondence estimators beyond DINOv3, or combining pseudo matches from multiple matchers, could further improve the quality and robustness of the correspondence supervision and generated results.

Sample [1/5]	Sample [1/5]	Sample [1/5]																																																																					
<p>Garment Text Annotation : Short sleeve white buttoned polo shirts with shirt collar neck</p>  <p>person garment (a) (b) (c)</p>	<p>Garment Text Annotation : Short sleeve white buttoned polo shirts with shirt collar neck</p>  <p>person garment (a) (b) (c)</p>	<p>Garment Text Annotation : Short sleeve white buttoned polo shirts with shirt collar neck</p>  <p>person garment (a) (b) (c)</p>																																																																					
<p>(1) Garment Transfer Consistency (GTC)</p> <p>For the generated images (a)–(c), please rate each image on a 1–5 scale based on the criteria below (1 = Very Poor, 5 = Excellent).</p> <ul style="list-style-type: none"> - How well the visual details of the garment—such as patterns, colors, and logos—are preserved and reflected. - How accurately the material appearance and texture of the garment are represented. <table border="1"> <thead> <tr> <th>1</th><th>2</th><th>3</th><th>4</th><th>5</th></tr> </thead> <tbody> <tr> <td>(a)</td><td><input type="radio"/></td><td><input type="radio"/></td><td><input type="radio"/></td><td><input type="radio"/></td><td><input type="radio"/></td></tr> <tr> <td>(b)</td><td><input type="radio"/></td><td><input type="radio"/></td><td><input type="radio"/></td><td><input type="radio"/></td><td><input type="radio"/></td></tr> <tr> <td>(c)</td><td><input type="radio"/></td><td><input type="radio"/></td><td><input type="radio"/></td><td><input type="radio"/></td><td><input type="radio"/></td></tr> </tbody> </table>	1	2	3	4	5	(a)	<input type="radio"/>	(b)	<input type="radio"/>	(c)	<input type="radio"/>	<p>(2) Textual Attribute Compliance (TAC)</p> <p>For the generated images (a)–(c), please rate each image on a 1–5 scale based on how well the garment reflects the attributes described in the Garment Text Annotation (1 = Very Poor, 5 = Excellent).</p> <table border="1"> <thead> <tr> <th>1</th><th>2</th><th>3</th><th>4</th><th>5</th></tr> </thead> <tbody> <tr> <td>(a)</td><td><input type="radio"/></td><td><input type="radio"/></td><td><input type="radio"/></td><td><input type="radio"/></td><td><input type="radio"/></td></tr> <tr> <td>(b)</td><td><input type="radio"/></td><td><input type="radio"/></td><td><input type="radio"/></td><td><input type="radio"/></td><td><input type="radio"/></td></tr> <tr> <td>(c)</td><td><input type="radio"/></td><td><input type="radio"/></td><td><input type="radio"/></td><td><input type="radio"/></td><td><input type="radio"/></td></tr> </tbody> </table>	1	2	3	4	5	(a)	<input type="radio"/>	(b)	<input type="radio"/>	(c)	<input type="radio"/>	<p>(3) Fit-Pose Consistency (FPC)</p> <p>For the generated images (a)–(c), please rate each image on a 1–5 scale based on the criteria below (1 = Very Poor, 5 = Excellent).</p> <ul style="list-style-type: none"> - How well the body structure (e.g., hands, arms, legs, hair) is preserved without distortion or disappearance. - How closely the overall pose matches that of the original Input Person image. - How naturally the garment fits the body of the person. <table border="1"> <thead> <tr> <th>1</th><th>2</th><th>3</th><th>4</th><th>5</th></tr> </thead> <tbody> <tr> <td>(a)</td><td><input type="radio"/></td><td><input type="radio"/></td><td><input type="radio"/></td><td><input type="radio"/></td><td><input type="radio"/></td></tr> <tr> <td>(b)</td><td><input type="radio"/></td><td><input type="radio"/></td><td><input type="radio"/></td><td><input type="radio"/></td><td><input type="radio"/></td></tr> <tr> <td>(c)</td><td><input type="radio"/></td><td><input type="radio"/></td><td><input type="radio"/></td><td><input type="radio"/></td><td><input type="radio"/></td></tr> </tbody> </table>	1	2	3	4	5	(a)	<input type="radio"/>	(b)	<input type="radio"/>	(c)	<input type="radio"/>																																				
1	2	3	4	5																																																																			
(a)	<input type="radio"/>	<input type="radio"/>	<input type="radio"/>	<input type="radio"/>	<input type="radio"/>																																																																		
(b)	<input type="radio"/>	<input type="radio"/>	<input type="radio"/>	<input type="radio"/>	<input type="radio"/>																																																																		
(c)	<input type="radio"/>	<input type="radio"/>	<input type="radio"/>	<input type="radio"/>	<input type="radio"/>																																																																		
1	2	3	4	5																																																																			
(a)	<input type="radio"/>	<input type="radio"/>	<input type="radio"/>	<input type="radio"/>	<input type="radio"/>																																																																		
(b)	<input type="radio"/>	<input type="radio"/>	<input type="radio"/>	<input type="radio"/>	<input type="radio"/>																																																																		
(c)	<input type="radio"/>	<input type="radio"/>	<input type="radio"/>	<input type="radio"/>	<input type="radio"/>																																																																		
1	2	3	4	5																																																																			
(a)	<input type="radio"/>	<input type="radio"/>	<input type="radio"/>	<input type="radio"/>	<input type="radio"/>																																																																		
(b)	<input type="radio"/>	<input type="radio"/>	<input type="radio"/>	<input type="radio"/>	<input type="radio"/>																																																																		
(c)	<input type="radio"/>	<input type="radio"/>	<input type="radio"/>	<input type="radio"/>	<input type="radio"/>																																																																		

Figure K.17. Example of User Study.

You are a strict virtual try-on (VTON) evaluator.

Given a person image **[IMG1]**, a garment product image **[IMG2]**, a generated try-on image **[IMG3]**, and a **GARMENT CAPTION**, determine TEXTUAL ALIGNMENT, VISUAL MATCH, FIT QUALITY, NON-TARGET INTEGRITY, and OVERALL SCORE.

Scoring Rules (continuous 0.0–5.0, discrete 1–5):

- TEXTUAL ALIGNMENT: adherence to caption attributes (category, sleeve length, neckline, material/signature)
- VISUAL MATCH: agreement with **[IMG2]** in silhouette, material, sleeve length, neckline, hem band, and reproduction of signature details
- FIT QUALITY: geometric/ratio-based naturalness vs intended fit (slim/regular/relaxed) using torso width ratio, sleeve wrist ratio, shoulder drop ratio, bunching level, contour loss %
- NON-TARGET INTEGRITY: preservation of non-target regions (hair/skin/hands/other clothes) and valid pose consistency
- OVERALL: mean of all scores, then limited by Visual and Fit

Category-Scoped Ignore Rule: Decide garment type from **[IMG2]+CAPTION** ∈ {TOP, BOTTOM, DRESS}.

From **[IMG1] → [IMG3]**, only that target garment category (TOP/BOTTOM/DRESS) may change .

All non-target regions must remain visually unchanged except minimal seam blending.

Hard Caps (applied after sub-scores):

- Category mismatch → TEXTUAL ≤2.0, VISUAL ≤2.0
- Length band mismatch (sleeve/hem) → TEXTUAL ≤2.0, VISUAL ≤2.0
- Silhouette mismatch → VISUAL ≤2.0
- Material/texture mismatch → VISUAL ≤2.0, FIT ≤3.0
- Missing essential signature detail → VISUAL ≤2.3, FIT ≤2.5
- If Visual silhouette component <0.6 or Visual_disc ≤2 → FIT ≤ VISUAL
- Severe artifacts → FIT ≤1.5
- Non-target changes → INTEGRITY ≤2.0, OVERALL ≤3.0

Caption Specificity Gate:

Caption explicitly containing ≥ 3 clothing attributes allows full (5.0) TEXTUAL score.

If only 1–2 attributes appear → cap TEXTUAL at 3.0–4.0.

Output Format (JSON only):

```
{
  "caption": "...",
  "garment_type": "TOP / BOTTOM / DRESS",
  "parsed_caption": ["category: ...", "sleeve: ...", "neckline: ...", "signature/material: ..."],
  "extracted_visual": ["silhouette: ...", "material/texture: ...", "signature: ...", "lower_length: ..."],
  "scores_continuous": { "textual": 0.0, "visual": 0.0, "fit": 0.0, "integrity": 0.0, "overall_continuous": 0.0 },
  "scores_discrete": { "textual": 1, "visual": 1, "fit": 1, "integrity": 1, "overall_discrete": 1 },
  "caps_applied": ["none"],
  "occlusions": ["none" | "..."],
  "reason": "<short numeric explanation>"
}
```

Figure K.18. Details on VLM Evaluation Prompt.